Behavioural Brain Research 428 (2022) 113884

Contents lists available at ScienceDirect

Behavioural Brain Research

journal homepage: www.elsevier.com/locate/bbr

Non-invasive in vivo MRI detects long-term microstructural brain alterations related to learning and memory impairments in a model of inflammation-induced white matter injury

Wyston C. Pierre [a,b], Erjun Zhang [a,d,e], Irène Londono [a], Benjamin De Leener [c,d], Frédéric Lesage [d,e], Gregory A. Lodygensky [a,b,e,*]

[a] Departments of Pediatrics, Ophthalmology and Pharmacology, CHU Sainte-Justine Research Centre, Montreal, QC, Canada
[b] Department of Pharmacology, Université de Montréal, Montreal, QC, Canada
[c] Department of Computer Engineering and Software Engineering, École Polytechnique de Montréal, Montreal, QC, Canada
[d] Institute of Biomedical Engineering, École Polytechnique de Montréal, Montreal, QC, Canada
[e] Montreal Heart Institute, Montreal, QC, Canada

ARTICLE INFO

Keywords:
Periventricular leukomalacia
Lipopolysaccharides
Fear conditioning
Diffusion tensor imaging
T2-weigthed imaging
In vivo high-field MRI

ABSTRACT

Magnetic resonance imaging (MRI) is currently under investigation as a non-invasive tool to monitor neurodevelopmental trajectories and predict risk of cognitive deficits following white matter injury (WMI) in very preterm infants. In the present study, we evaluated the capacity of multimodal MRI (high-resolution T2-weighted imaging and diffusion tensor imaging)to assess changes following WMI and their relationship to learning and memory performance in Wistar rats as it has been demonstrated for preterm infants. Multimodal MRI performed at P31-P32 shown that animals exposed to neonatal LPS could be classified into two groups: minimal and overt injury. Animals with overt injury had significantly enlarged ventricles, hippocampal atrophy, diffusivity changes in hippocampal white and gray matter, in the striatum and the cortex. Following neonatal LPS exposure, animals presented learning and memory impairments as shown at the fear conditioning test at P36-P38. The severity of learning and memory deficits was related to increased mean diffusivity in the hippocampal region. In conclusion, non-invasive multimodal MRI (volumetric and DTI) assessed and classified the extent of injury at long-term following neonatal LPS exposure. Microstructural changes in the hippocampus at DTI were associated to learning and memory impairments. This further highlights the utility of multimodal MRI as a non-invasive quantitative biomarker following perinatal inflammation.

1. Introduction

Preterm born infants are at high risk of neurodevelopmental impairments following exposure to sterile and/or infectious inflammatory episodes during the perinatal period. Using MRI, it was found that more than 70% of very preterm (VP) infants (born <32 weeks or very low birthweight < 1250 g) suffered from diffuse white matter injury (WMI) [1,2]. Within this population, up to 50% are at risk of adverse long-lasting neurodevelopmental outcomes including cognitive and behavioral deficits, attentional defects and learning and memory impairments [3–5].

MRI is a powerful tool to assess brain developmental trajectories in preterm neonates by allowing early detection of brain injuries and long-term follow-up studies [6,7]. On volumetric MRI, VP infants exhibited altered growth rates, delayed maturation, and lower volume in different cerebral regions, particularly in the hippocampus, compared to term-born infants [8–11]. It was established that the hippocampal atrophy persisted up to early adulthood and increased the risk of learning

Abbreviations: AD, Axial diffusivity; DBSI, Diffusion basis spectrum imaging; dMRI, Diffusion MRI; DTI, Diffusion tensor imaging; DWI, Diffusion weighted imaging; FA, fractional anisotropy; LPS, Lipopolysaccharides; MD, Mean diffusivity; MRI, magnetic resonance imaging; MRS, Magnetic resonance spectroscopy; NODDI, Neurite orientation dispersion and density imaging; SEMS, Spin-echo multi-slice; SNR, Signal-to-noise ratio; RD, Radial diffusivity; VP, Very preterm; WMI, White matter injury.

* Correspondence to: Department of Pediatrics, NICU, Sainte-Justine Hospital and Research Center, 3175 Chemin de la Côte Sainte-Catherine, Montreal, QC H3T 1C5, Canada.

E-mail address: ga.lodygensky@umontreal.ca (G.A. Lodygensky).

https://doi.org/10.1016/j.bbr.2022.113884
Received 4 November 2021; Received in revised form 18 March 2022; Accepted 3 April 2022
Available online 6 April 2022

and memory impairments [12–17]. Furthermore, long-lasting alterations in cortical thickness and/or organization were also associated with memory impairments observed in VP infants [18,19].

Diffusion tensor imaging (DTI), an MRI technique based on anisotropic diffusion, allows in vivo assessment of white and gray matter microstructure integrity and maturation during neurodevelopment [20–22]. The use of serial DTI acquisitions recently showed that gray and white matter had similar maturation rates, which could be affected by preterm birth and presence of WMI [23,24]. Compared to term infants, preterm neonates exhibited changes in diffusivity in different white matter fibers, particularly the corpus callosum, that persisted up to early adulthood and in these cases, the alterations correlated to long-term deficits including memory and learning impairments [25–29]. These microstructural alterations in the white matter reflected deficits in myelination, axonal integrity, and brain connectivity [30,31]. Likewise, DTI performed at term equivalent age showed that preterm infants had a more immature cortical development compared to term infants, which was characterized by an increased mean diffusivity [24,32]. Although it is still under investigation, it was posited that gray matter diffusivity changes could reflect alterations in cellular complexity, synaptogenesis, and neurite growth [32–34]. Furthermore, DTI is an interesting tool for early evaluation of therapeutic response in both clinical and preclinical research. Clinical DTI allowed in vivo assessment of injury progression and efficacy of therapeutic interventions in pediatric central nervous system tumors [35–37], adult and pediatric stroke [38–41], and depressive disorders in adults [42–44]. DTI detected the neuroprotective response of different experimental molecules on animal models of neonatal WMI such as following LPS exposure or hypoxia-ischemia [45–48]. The increasing use of DTI in both clinical and preclinical research pinpoints the need to define its capacity to evaluate ongoing neuroinflammatory injury in the developing brain.

A robust model of inflammatory WMI consists of intracerebral injection of lipopolysaccharides (LPS) in the corpus callosum of 3–5-day-old rats during an age period where the rat brain is equivalent to a preterm infant's brain [49–51]. This model mimics multiple pathophysiological changes seen in VP infants with WMI such as gliosis, ventricular dilatation, hypomyelination and late hippocampal atrophy [48–50,52–56]. As ventricle dilation is a well-established hallmark of WMI, our previous studies showed the presence of variability in extent of injury at 21 days following neonatal LPS exposure with a subgroup of animals presenting highly dilated ventricles [54]. Similar to neurodevelopmental impairments seen in neonates with WMI, this animal model exhibited behavioral alterations including motor deficits, hyperactivity, less anxiety-like behaviors and learning and memory impairments [57–60]. Moreover, this model exhibited changes on MRI similar to the pathophysiological hallmarks seen in VP infants with WMI. During the acute phase of inflammation (24 h post injury), this model had diffusivity restriction that correlated to increased apoptosis, astrogliosis and microglia activation [48,61]. Using magnetic resonance spectroscopy (MRS), we have previously shown that hippocampus metabolism was altered during the early phase of inflammation (24 h post-injury) that preceded the known axonal injury and hippocampal atrophy that appears at later in this animal model [48,56,57]. Although long-term behavioral and histopathological changes are well understood in this animal model, little is known on long-term changes on MRI and their relationship to pathophysiological processes. Currently, the majority of the long-term animal studies using LPS-induced WMI model evaluated neuropathological changes using post-mortem analysis with very few using in vivo evaluation of injury progression. Thus, there is a need to assess these long-lasting neurological alterations with non-invasive in vivo biomarkers particularly in the context of neurodevelopment.

The aim of this study was to evaluate the capacity of DTI and volumetric MRI to assess the extent of injury at 4 weeks after neonatal exposure to LPS and whether the imaging biomarkers correlated with learning and memory impairments in this animal model.

2. Methods and materials

2.1. Animal preparation

All animal-handling procedures were approved by the Institutional Committee for Animal Care of the Montreal Heart Institute Research Center, following the recommendations of the Canadian Council of Animal Care. The animals were given ad libitum access to water and food and were exposed to 12 h light/ dark cycles. Similar to our previous studies, only male rats were used in this study to limit results variability related to animal sex [48,62].

2.1.1. Intracerebral injection

Six litters of male Wistar rat pups with dam (6–8 pups per litter) were obtained from Charles River (Charles River, QC, Canada). A total of 22 three-days-old (P3) male Wistar rats were randomly assigned to the Sham group (n = 10) or to the LPS group (n = 12) with each litter having at least 2 animals from each treatment group. At the time of the intracerebral injection, pups in the Sham group had an average body weight of 9.41 ± 0.34 g and LPS pups weighted 9.43 ± 0.32 g. The LPS group received an intracerebral injection of a suspension of 16 μg/μl LPS (1 mg/kg Lipopolysaccharide E. coli, serotype 448 055:B5, SigmaAldrich, Oakville, ON, Canada), in sterile saline (0.5 μl for 8 g pup). An equivalent volume of 0.9% sterile saline solution alone was injected to the Sham pups. The intracerebral injection was made in the left corpus callosum at a level equivalent to P-7, c9 [63] under ultrasound guidance using Vevo LAZR micro-ultrasound system (FUJIFILM VisualSonics Inc., Toronto, ON, 457 Canada) as previously published (See supp. Fig. 1) [48,61]. A micropipette mounted on a microprocessor-controlled injector (Micro4 from World Precision Instruments, Sarasota, FL, USA) with a rate of 100 nL/min was used for the injections. All the injections were performed under isoflurane anesthesia. The pups were placed on a thermal blanket for recovery and before being returned to their dam. The pups were weaned at P21 and were housed in standard polypropylene cages with four rats per cage. Brain MRI was done at P31-P32 and behavioral testing was performed at P36-P38.

2.2. Magnetic resonance imaging

All MRI experiments were acquired on an actively shielded 7 T/ 30 cm horizontal bore magnet scanner interfaced with a DirectDrive console (Agilent, Palo Alto, CA, USA) with gradients of 600 mT/m as previously described [48,52]. For MRI acquisition, rats were anesthetized with isoflurane (3% for induction; 0.5–2% for maintenance) [64]. Physiological monitoring (body temperature and respiration rate) was conducted with a custom-built pressure pillow combined with a temperature probe placed under the abdomen. Temperature was maintained stable at 36.0 °C using a warm air fan (SA Instruments, Stony Brook, NY, USA). Respiration was maintained around 75 breaths/min by adapting the level of isoflurane.

At 4 weeks following the intracerebral LPS injection (P31-P32), T2-weighted images and diffusion weighted imaging (DWI) were acquired on Sham (n = 10)and LPS (n = 12) animals with an average body weight of 136.9 ± 6.27 g and 126.5 ± 3.03 g respectively. P31-P32 rat brain corresponds to the neurodevelopmental period of school-aged children (9–11 years old) [51,65]. Multimodal MRI acquisitions were conducted using a receive only surface coil positioned over the rat brain and in combination with a quadrature transmit birdcage coil with an internal diameter of 69 mm as previously published (Rapid Biomedical, Germany) [64,66]. T2-weighted images of the whole brain were acquired using true fast imaging with steady-state precession (true FISP) sequence with repetition time (TR) = 4.6 *ms*, echo time (TE) = 2.3 *ms*, a $133\ \mu m^3$ isotropic resolution and a field of view (FOV) of 24 *mm* × 20 *mm* × 15 *mm*. The total acquisition time was 5 min per animal. Coronal DWI of the entire brain were acquired using a dual spin-echo multi-slice (SEMS) imaging sequence with TR = 1800 *ms* and TE = 35

ms. Diffusion-weighted volumes ($\delta = 7$ *ms*; $\Delta = 21$ *ms*; $b = 900$ *s/mm*^{2}) were acquired in two sets of 6 non-collinear directions applied in origin-symmetric fashion. Data were acquired with an acquisition matrix of 128 × 64 over 25 slices, and with a native resolution of 141 μm × 234 μm × 800 μm. The total acquisition time was 54 min per animal.

2.2.1. Volumetric measurements of the lateral ventricles and the hippocampus

The lateral ventricles and hippocampi were manually segmented on T2-weighted coronal slices using Fiji [67]. The volume (mm^3) of each structure was computed by summing the size of the evaluated 2D areas multiplied by the slice thickness (0.133 mm).

2.2.2. DTI preprocessing and analysis

Fractional anisotropy (FA), radial diffusivity (RD), axial diffusivity (AD), mean diffusivity (MD) and color-coded (Red, Green and Blue - RGB) FA maps were reconstructed by using the RESTORE algorithm for robust tensor fitting offered by DIPY [68,69]. Using the tensor-based template buildup tool implemented in DTI-TK [70,71], we created our own population-specific template to reduce potential biases. First, all DWI images were resampled to *128 × 128 x 32* (*141 μm x 141 μm x 800 μm*). To ensure a good quality template, outliers were removed by setting the threshold (≥ 0.05 μm^2/ms) of the main direction diffusivity coefficient and signal isolated voxel were removed by using median OTSU masking method [69]. Then, the five images with the highest signal-to-noise (SNR) and normal brain morphology were chosen and were treated and averaged as the initial template. Next, the five chosen diffusion tensor images were used to update the initial template through three rigid registration iterations, three affine iterations and six diffeomorphic iterations with a threshold on the convergence of 0.002. The template was updated after each iteration by averaging the normalized images. All steps were conducted using the Euclidean Distance Squared between tensors as a metric. Since we used young rat brains in this project, the species of DTI-TK was set as RAT [70] and the length scale for piecewise affine deformation was decreased to 0.05 mm [52]. After creating the template, all the rat brains were registered to the template following the above registration steps (three rigid registration iterations, three affine iterations and six diffeomorphic iterations) without updating the template. The registration results were visually checked to confirm proper alignment.

In this study, a total of 15 regions of interest (ROIs) were manually delineated on the color-coded FA map derived from the brain template. ROIs were placed on the corpus callosum, on the ipsilateral and contralateral fimbria, the ipsilateral and contralateral hippocampus (subdivided into the CA1, CA2/CA3 and dentate gyrus areas), on the ipsilateral and contralateral dorsal striatum and on the ipsilateral and contralateral cortical region encompassing the retrosplenial and motor cortex. The corpus callosum and fimbria were chosen as they were connected to long-lasting memory impairments in preterm-born individuals [18,19,72,73]. The hippocampus was selected as it is highly vulnerable, particularly the CA1 region, to adverse insults in both human and rodents [56,74–77]. The dorsal striatum was selected as it was shown to be altered following neonatal LPS exposure [60,61]. Moreover, ROIs were also placed on the ipsilateral and contralateral retrosplenial and motor cortex as we previously showed altered connectivity patterns in these regions following neonatal LPS exposure [78]. The selected ROIs were also overlaid on the registered maps of the subjects to visually check if the ROIs were positioned on the right regions for each subject. In our results, one rat brain failed the registration process due to presence of significant anatomic deformations. For this brain failing registration, the ROIs were drawn manually on its color-coded FA map. After the data preprocessing, averaged diffusivity values (AD, RD, MD, and FA) in each ROI of each brain were calculated. In order to access cortical microstructural changes, principal diffusion direction vectors were displayed over the FA maps by using FSL tool [79].

2.3. Fear conditioning test

Memory and learning processes were assessed by performing a fear conditioning test at P36-P38 which is equivalent to human early adolescent neurodevelopment (12–14 years old) [51,65]. Furthermore, P36–38 was chosen as rats aged over P24 exhibit mature freezing behavior during the fear conditioning test [80]. The apparatus includes a cage with an electrified grid floor contained in a soundproofed cubicle with speakers and dimmed lighting (6.4 lux) (Harvard Apparatus). The test was done over 3 days. On day 1 (P36), the rats were placed inside the cage for 5 min to acclimate. On day 2 (P37), the animals were placed in the cage for 5 min, during which time they heard a non-aversive sound (2 kHz, 60 dB, 2 s) followed by an electrical shock (0.5 mA for 2 s) that were presented at 2 min and 4 min. This allowed the rats to learn that the sound (conditioned stimulus) is coupled to an electrical shock (unconditioned stimulus) [81,82]. On day 3 (P38), the rats were submitted to a test session during which they were placed in the setup for 5 min, with the sound occurring alone at 2 min and 4 min. The setup was cleaned with 70% ethanol between each animal at each day of behavioral testing. Freezing behavior was used as a measure of fear memory and learning and was defined as the percentage of time spent in complete absence of all movement except that required for respiration [83,84]. Freezeframe software (Actimetrics, Wilmette, IL, USA) was used to deliver tones and shocks and to perform unbiased behavioral analysis of freezing behavior [85].

2.4. Statistical analysis

All statistical tests were done using the GraphPad Prism 9.1.0 software (GraphPad Software, La Jolla, CA) and statistical significance was set at P-value < 0.05. We tested for normal distributions using the Shapiro-Wilk test. For the analysis of MRI data, outlier values were removed using the ROUT method with Q = 0.5% [84]. MRI data (volumetric measure and DTI) were analyzed using Kruskal-Wallis test followed by Dunn's multiple comparisons test. All MRI data are presented as median ± 95% confidence interval (CI). Freezing behavior data during the different sessions of fear conditioning were analyzed with 2-way ANOVA (time and group) with Dunnett post hoc test for selected comparisons. Freezing behavior data are presented as mean ± SEM.

3. Results

3.1. Volumetric measurement on T2-weighted images

Ventriculomegaly at *ex vivo* MRI and post-mortem histology is a well-established pathophysiological hallmark in this animal model [49,52,54,78]. The hippocampus is known to undergo late atrophy following WMI in human and in this animal model [12,13]. Based on the presence of visually discernable ventriculomegaly following qualitative analysis of T2-weighted images, LPS exposed animals were further separated into two subgroups: LPS (Min. injury) = 9 and LPS (Overt injury) = 3.

3.1.1. Neonatal LPS exposure induces ventricular dilatation

Knowing that lateral ventricle enlargement is the most common histopathological hallmark in LPS-injected rats, we measured lateral ventricles volume on T2-weighted images acquired at P31/32 (Fig. 1 A). Compared to Sham animals, LPS animals with minimal brain injury had non-significative bilateral ventricle dilation which represented ≈ 19% increase in total lateral ventricles volume (3.485 ± 0.21 vs 4.159 ± 0.183 mm^3 respectively, *P value* = 0.179) (Fig. 1 B). LPS rats with overt injury presented more than 100% bilateral increase in lateral ventricles volume that was statistically significant compared to Sham animals (3.485 ± 0.21 vs 69.580 ± 25.44 mm^3 respectively, *P value* = 0.003) (Fig. 1 B). Thus, neonatal LPS exposure resulted in bilateral ventriculomegaly which reached statistical significancy in a subgroup of

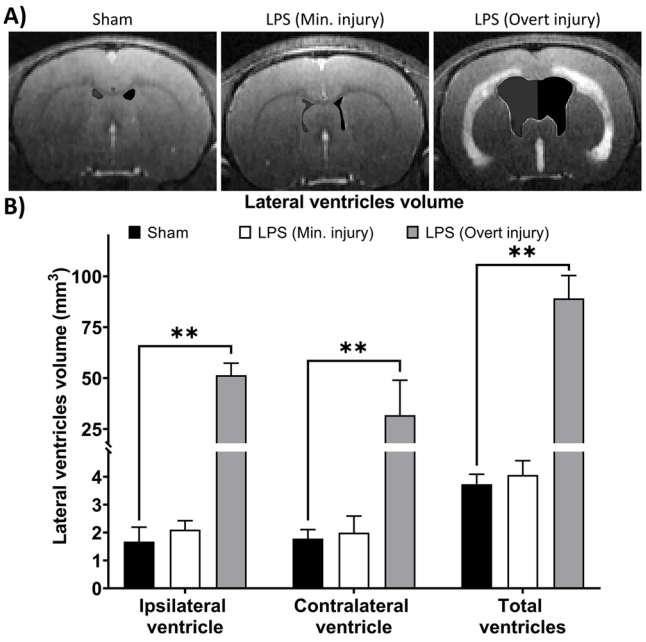

Fig. 1. Lateral ventricles volume measured on coronal T2-weighted images acquired at P31-P32. (A) Representative images of lateral ventricles in animals of each group. The ROI overlay depicts the ipsilateral side in gray and the contralateral side in black. (B) Bar graph of quantification of lateral ventricles volume on T2-weighted images. Note the significant bilateral ventricular dilatation in LPS animal with overt injury (LPS Overt injury). Values are represented as median ± 95% CI. * * $p < 0.01$ compared to Sham.

highly injured animals.

3.1.2. Neonatal LPS exposure is associated to hippocampal atrophy

We investigated changes in hippocampus volume on T2-weighted images (Fig. 2 A) in the animals exposed to neonatal LPS. We found that there was no statistically significant difference in hippocampus volume between Sham and LPS (Min. injury) group (Fig. 2). The LPS

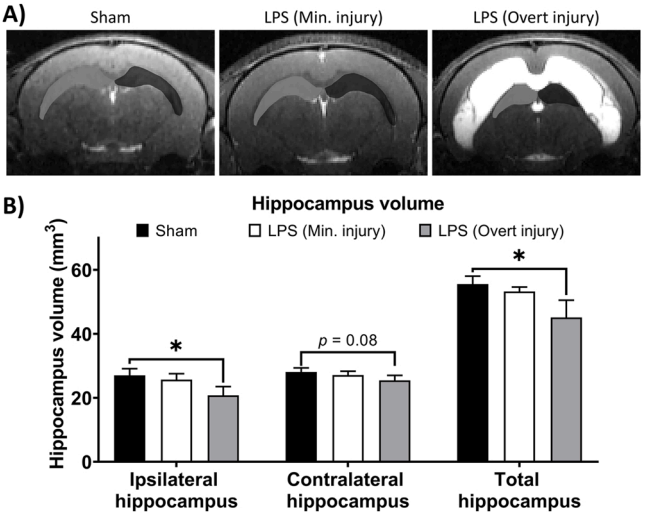

Fig. 2. Hippocampus volume measured on coronal T2-weighted images acquired at P31-P32. (A) Representative images of hippocampus from each group of animals. The ROI overlay depicts the ipsilateral side in light gray and the contralateral side in black. (B) Bar graph of hippocampus volume on T2-weighted images for ipsilateral hippocampus, contralateral hippocampus, and total hippocampus. Note the significant hippocampal atrophy in LPS animal with overt injury (LPS Overt injury). Values are represented as median ± 95% CI. *$p < 0.05$ compared to Sham.

(Overt injury) animal showed significant reduction (≈13% reduction) in the ipsilateral hippocampus volume (Fig. 2 B) and the total volume of hippocampus (Fig. 2 B) compared to Sham animals. There was a trend toward reduced contralateral hippocampus volume between Sham and LPS (Overt injury) animals (27.96 ± 0.64 vs 25.39 ± 0.95 mm^3 respectively, *P value* = 0.0836) (Fig. 2 B). In order to determine if the extent of ventricle dilatation was associated to hippocampus atrophy, we applied a linear regression analysis which demonstrated indeed a highly significant relationship between the lateral ventricles volume (LVvol) and the total volume of hippocampus (HCvol):

$$\ln(\text{HCvol}) = -0{\cdot}049 \times \ln(\text{LVvol}) + 4{\cdot}042;\ \boldsymbol{R^2 = 0.392},\ P = 0.002{\cdot}$$

Thus, LPS (Overt injury) animals in the present study are characterized by the presence of ventriculomegaly and concurrent hippocampal atrophy.

3.2. Neonatal LPS exposure leads to memory and learning impairments

To assess the presence of learning and memory impairment following neonatal LPS exposure, we performed at P36-P38 a fear conditioning test in which a conditioned stimulus (sound) is paired to an unconditioned stimulus (shock) (Fig. 3 A). The efficiency of learning and memory is portrayed by an increased freezing behavior during conditioning and test sessions. During the habituation period, animals exhibited very low freezing behavior that was not significantly different between the groups (Fig. 3 B). Two rats in the Sham group exhibited abnormally low levels of freezing during conditioning (> 2 standard deviation from the mean) and were excluded from further analysis accordingly to previous studies [86–90]. During the conditioning session, the freezing value increased following the first sound-shock coupling in the Sham group. The LPS (Min. injury) animals had increased freezing percentage to a similar extent than Sham animals (Fig. 3 C). The LPS (Overt injury) group had lower freezing behavior following the first sound-shock coupling compared to Sham and LPS (Min. injury) groups that reached statistically significance at the 180–240 s interval (Fig. 3 C).

During the test session, Sham animals showed increased freezing behavior particularly after the first sound which indicates proper learning and memory processes (Fig. 3 D). LPS (Overt injury) animals showed the lowest amount of freezing behavior compared to Sham group that was significant as early as after the first sound (120–180 s interval) (Fig. 3 D). Compared to Sham animals, LPS (Min. injury) had a shorter freezing behavior that reached statistical significance only after the second sound (Fig. 3 D). Combined together, these results indicate that learning and memory processes deficits increase with the extent of brain injury in neonatal LPS-induces WMI.

3.3. Neonatal LPS exposure alters DTI-defined microstructure in the hippocampus white and gray matters

DTI was acquired on 22 animals (10 Sham, 9 LPS (Min. injury) and 3 LPS (Overt injury)) to measure fractional anisotropy (FA), mean diffusivity (MD), axial diffusivity (AD) and radial diffusivity (RD) in the central part of the corpus callosum and in the ipsilateral and contralateral fimbria and hippocampus subdivisions (Figs. 4 A and 5 A). Using the ROUT method, diffusivity values of one Sham animal were excluded as it was considered as an outlier due to poor SNR, thus only 9 Sham animals were used in DTI analysis.

There were no significant differences in FA between groups in the corpus callosum and the ipsilateral and contralateral fimbria (Fig. 4). No significant difference in all diffusivity parameters (MD, AD and RD) in the corpus callosum and the ipsilateral and contralateral fimbria was observed between Sham and LPS (Min. injury) animals (Fig. 4). Animals in the LPS (Overt injury) group had significant increase in MD, AD and RD in the corpus callosum and ipsilateral fimbria compared to Sham

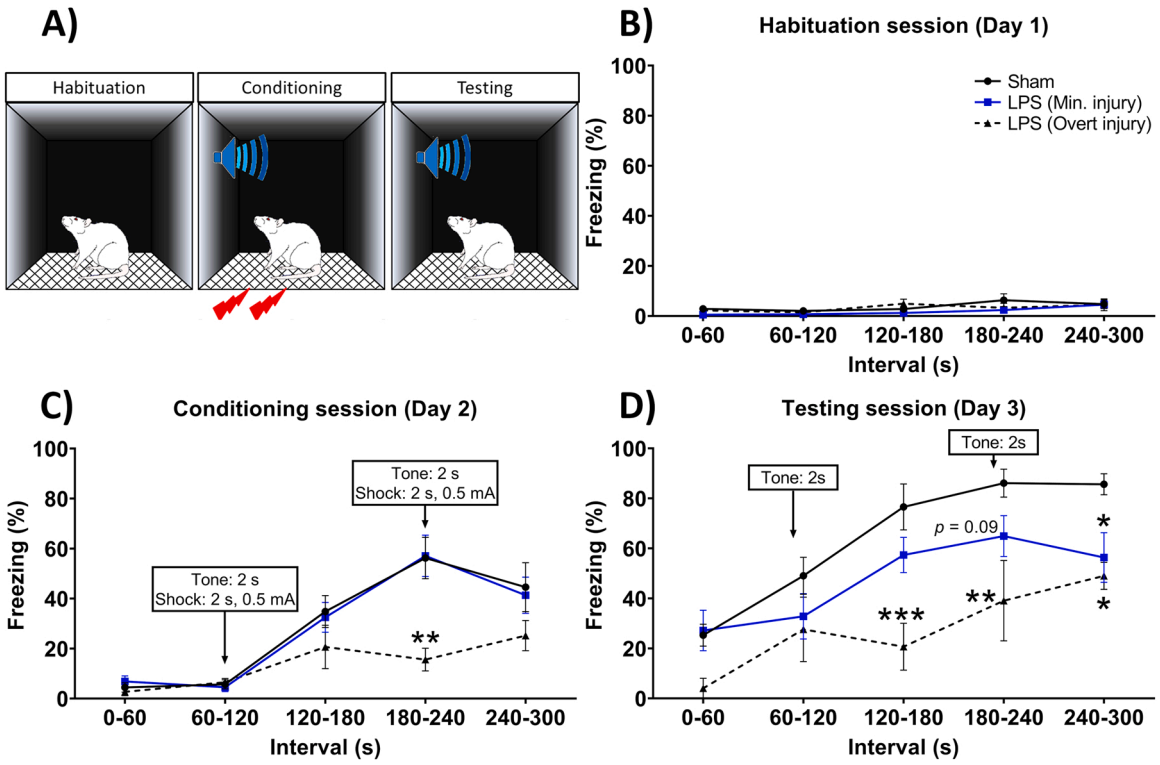

Fig. 3. Effect of neonatal LPS exposure on learning and memory at P36-P38. (A) Schematic of a rat in the fear conditioning apparatus. Chart of averages over 60 s of percentage of freezing behavior during (B) Habituation session; (C) Conditioning session in which a shock is coupled to a sound and (D) Testing session where the animal is only presented the sound. Values are represented as mean ± SEM. * $p < 0.05$; ** $p < 0.01$; ** $p < 0.001$ compared to Sham.

group (Fig. 4 B and C). Compared to LPS (Min. injury), animals in the LPS (Overt injury) had increased MD in the ipsilateral fimbria (Fig. 4 C).

There were no significant changes in diffusivity parameters (MD, AD and RD) in all the between Sham and LPS (Min, injury) in all the hippocampal subdivisions (Fig. 5). No significant changes in FA between the groups were observed (Fig. 5) except a decrease in FA in the contralateral CA2/CA3 in LPS (Overt injury) animals compared to Sham (Fig. 5 E). Animals with overt injury presented significant increase in MD, AD and RD in the ipsilateral CA1 region compared to Sham animals (Fig. 5 B). LPS (Overt injury) group had increased MD and RD compared to Sham group in the ipsilateral CA2/CA3 region (Fig. 5 D). Compared to Sham group, animals with overt injury showed significant increase in RD in the contralateral CA1 and CA2/CA3 regions (Fig. 5 C and E). Compared to LPS (and Min. injury), animals in the LPS (Overt injury) had significant increase in MD in the ipsilateral CA1 and CA2/3 regions and increased RD in the ipsilateral CA1, CA2/CA3 and dentate gyrus subdivision (Fig. 5 B, D and F).

Knowing that the fimbria and the CA1 region partakes in learning and memory processes, we looked at the possibility that changes in mean diffusivity would identify animal performance at P38 during the fear conditioning testing session at the 180–240 s interval (Fig. 3 D). We found a significant linear regression between ipsilateral fimbria mean diffusivity and the percentage of freezing at the 180–240 s interval:

$$\%\ \text{of freezing} = -46{\cdot}60 \times \text{MD}_{\text{ipsilateral fimbria}} + 106{\cdot}9;\ \boldsymbol{R^2 = 0.330};\ P = 0.010{\cdot}$$

There was also a significant relationship between mean diffusivity in the ipsilateral CA1 region and freezing behavior at 180–240 s interval:

$$\%\ \text{of freezing} = -71{\cdot}23 \times \text{MD}_{\text{ipsilateral CA1}} + 125{\cdot}3;\ \boldsymbol{R^2 = 0.304};\ P = 0.014{\cdot}$$

3.4. Neonatal LPS exposure induces alteration in the striatum and the cortex

As previous studies showed that LPS exposure led to acute alteration of diffusivity in the striatum with increased apoptosis and lost-lasting decreased striatum volume [60,61], we measured diffusivity changes in the ipsilateral and contralateral dorsal striatum (Fig. 6 A). There was no significant difference in MD, RD and FA between the groups in the ipsilateral and contralateral dorsal striatum (Fig. 6 C and D). Compared to the Sham group, animals in the LPS (overt injury) group had significant increase in AD in the ipsilateral striatum and a trend toward increased AD in the contralateral striatum ($p = 0.05$).

In light of the qualitative appearance of reduced cortical thickness on T2 weighted images of severely injured animal and on the long-lasting cortical alterations reported in this animal model [53,78], we looked at the presence of cortical alterations on DTI performed at P31–32 following neonatal LPS exposure (Fig. 6 B). We observed that LPS (Overt Injury) had a trend toward increased RD compared to Sham ($p = 0.07$) and this increase in RD was statistically significant against the LPS (Min. Injury) group in the ipsilateral cortical region (Fig. 6 E). There was no significant change in FA, MD and AD between the groups in the ipsilateral cortex (Fig. 6 E). We did not detect any significant alteration in diffusivity in the contralateral cortex (Fig. 6 F).

4. Discussion

In the present study, multimodal MRI (T2 weighted and DTI) identified animals exposed to neonatal LPS with minimal injury from ones with overt injury. The severity of learning and memory impairments increased with extent of injury seen with non-invasive MRI. Animals with minimal injury had no significant difference on quantitative measures performed with multimodal MRI compared to Sham animals and exhibited subtle signs of memory impairments during fear conditioning test. Animals with overt injury displayed signs of severe memory

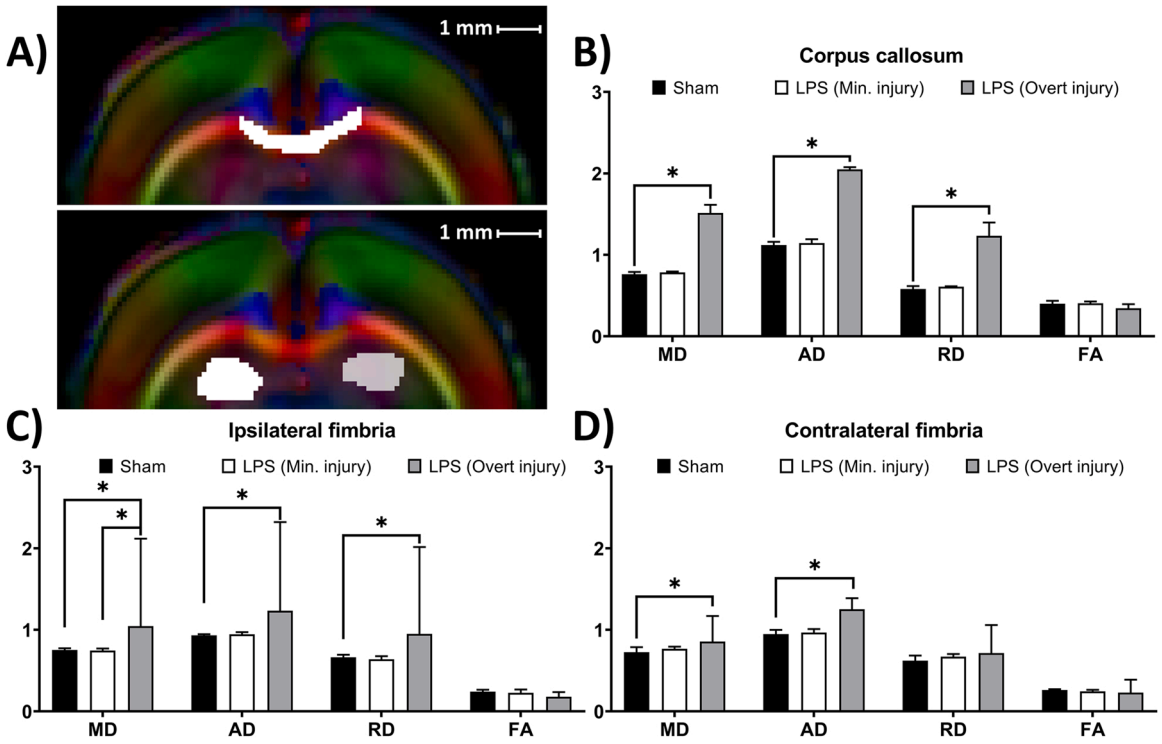

Fig. 4. *In vivo* diffusion tensor imaging acquired in P31-P32 rats exposed to neonatal LPS. (A) Examples of coronal RGB (red, green, and blue) map with the highlighted ROIs (the corpus callosum and the ipsilateral and contralateral fimbria. The ROI overlay depicts the ipsilateral side in white (left side) and the contralateral side in gray (right side). The colors in the RGB map represent the preferred direction of water diffusion. Red corresponds to medial-lateral, green to superior-inferior, and blue to rostral-caudal directions. Bar graph of mean diffusivity (MD), axial diffusivity (AD), radial diffusivity (RD) and fractional anisotropy in the (**B**) corpus callosum, (**C**) ipsilateral fimbria, and (**D**) contralateral fimbria. Values are represented as median ± 95% CI. * $p < 0.05$ compared to Sham or LPS (Min. injury). Diffusivity values (MD, AD and RD) are in: $\mu m^2 \cdot ms^{-1}$. (For interpretation of the references to colour in this figure legend, the reader is referred to the web version of this article.)

impairments and they presented ventriculomegaly, hippocampal atrophy, and increased diffusivity (AD, RD, and MD) especially in the hippocampus. Additionally, increased AD in the dorsal striatum and subtle nonsignificant increased RD in the retrosplenial and motor cortices were seen in animal with overt injury. Interestingly, increase in mean diffusivity in the ipsilateral CA1 region and fimbria were associated with a reduction in freezing behavior during the fear conditioning test.

The presence of variability in severity of LPS-induced injury could be due to interindividual variability present in rodents [91–93]. It was shown in animal model of traumatic brain injury and neonatal hypoxia-ischemia that neurological injury progression and intensity differed between animals [94–96]. Although the mechanisms leading to interindividual differences are not well understood, it was posited that they could result from difference in the epigenetic landscape [91,97]. In a previous study, we demonstrated that the methylation level of several genes related to inflammation and myelination differed between animals exposed to intracerebral LPS [54]. Furthermore, the variability in the response to LPS started as early as during the acute phase of injury [54,98]. As injury severity progression can differ between animals, it is important to take in consideration the presence of this variability in animal models particularly when testing for neuroprotective molecules.

Consistent with previous studies, neonatal LPS exposure induced memory and learning impairments at P36-P38 during the fear conditioning test with the deficit's severity increasing with extent of injury [55,60,99,100]. In our study, animals with overt WMI had difficulties to associate tone-shock pairing during the conditioning session and consequently, these animals had poorer performance during the testing session. During the fear conditioning test, learning and memory processes require proper connective integrity between different brain areas including the hippocampus and cortical regions such as the retrosplenial cortex [84,101–103]. The lack of learning in the animal with overt injuries could result from the alterations in the hippocampal region and the retrosplenial region as seen with multimodal MRI. The alteration in learning following neonatal LPS exposure was also seen during the step-down passive avoidance test, which assesses learning and memory, as animals with WMI required more electric shock to learn to stay on the platform and they presented poorer performance when tested 24 h later [55,60,100]. Although animals with minimal injury associated tone to shock to a similar extent than Sham animals, they displayed decreased freezing behavior during the testing session. If confirmed in future studies, these results would suggest that fear conditioning testing represent a robust and sensitive behavioral assay to discriminate learning and memory performance depending on the extent of WMI between animals.

Volumetric analysis of T1- and T2-weighted MRI acquisitions is used to detect subtle changes in neurodevelopmental trajectory in preterm infants [8]. In accordance to previously published data in humans and animals WMI, T2-weighted volumetric assessment showed that severely injured animals had overt ventriculomegaly and hippocampal atrophy at 28 days post-injury (P31-P32) [4,15,49,52,56,104]. Although not significant, a subtle increase in lateral ventricle volume was present in animal with minimal injury. The mechanisms leading to this increase are not fully well understood; however, it was posited that ventricular dilatation could result either from loss of tissue or from increased intraventricular pressure following intraventricular hemorrhage [105–109]. As moderate or severe intracerebral hemorrhage is a rare occurrence in our animal model, the ventricular dilatation should be mostly induced by loss of tissue in the periventricular area [110]. Interestingly, the increase in lateral ventricle volume was associated to hippocampal atrophy in our study. In a recent study, the hippocampal atrophy was associated to lateral ventricle dilatation in preterm infants with severe encephalopathy and the changes in hippocampal volume

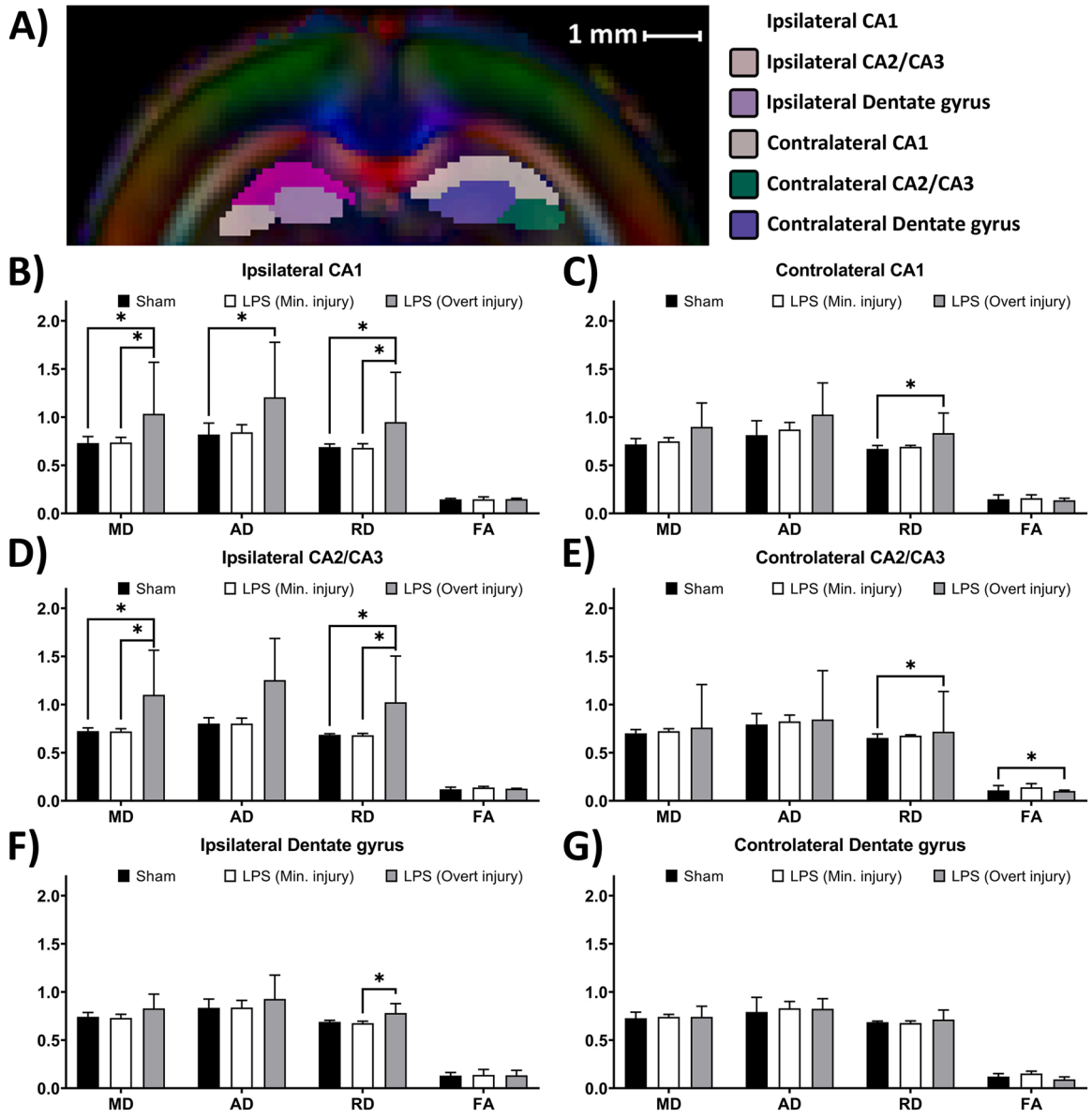

Fig. 5. *In vivo* diffusion tensor imaging of the hippocampus acquired in P31-P32 rats exposed to neonatal LPS. (A) Example of coronal RGB (red, green, and blue) map with the highlighted ROIs of the different hippocampus subdivisions. The ROI overlay depicts the ipsilateral side in white (left side) and the contralateral side in gray (right side). The colors in the RGB map represent the preferred direction of water diffusion. Red corresponds to medial-lateral, green to superior-inferior, and blue to rostral-caudal directions. Bar graph of mean diffusivity (MD), axial diffusivity (AD), radial diffusivity (RD) and fractional anisotropy in the (B) Ipsilateral CA1 region, (C) Contralateral CA1 region, (D) Ipsilateral CA2/CA3 region, (E) Contralateral CA2/CA3 region, (F) Ipsilateral Dentate gyrus and (G) Contralateral Dentate gyrus. Values are represented as median ± 95% CI. * $p < 0.05$ compared to Sham or LPS (Min. injury). Diffusivity values (MD, AD and RD) are in: $\mu m^2 \cdot ms^{-1}$. (For interpretation of the references to colour in this figure legend, the reader is referred to the web version of this article)

correlated to poorer cognitive performance at 2 years of age [111]. Moreover, it was suggested that lateral ventricle dilation could accentuate hippocampal atrophy by activating several deleterious pathways including increased inflammatory response [111,112]. Thus, ventricular dilatation might not solely be a consequence of periventricular tissue loss, but it could also accentuate the vulnerability of surrounding cerebral regions. Our results further highlight the need for a better understanding of pathophysiological mechanisms linking these two central hallmarks of neonatal WMI.

DTI allows non-invasive assessment of microstructural changes during physiological and pathological neurodevelopment in both white and gray matter in the brain. Using in vivo DTI at P31-P32, we showed that rats with overt brain injury following neonatal LPS exposure had increased diffusivity (MD, AD and RD) in the corpus callosum and within the fimbria (white matter tract) and the CA1 region (gray matter) of the hippocampus. These changes in LPS exposed animals are consistent with previous research which found that preterm birth and WMI were associated to increase in MD values driven mainly by changes in RD [113–116]. Moreover, analysis of hippocampus subdivision showed that CA1 region of the hippocampus had greater diffusivity alterations compared to the CA2/CA3 or the dentate gyrus subdivision. This is in accordance with the with studies in VP born adolescents that showed enhanced vulnerability of CA1region compared to other hippocampus subdivisions [76,77]. The increase in MD, AD and RD observed in the corpus callosum, the ipsilateral fimbria and the CA1 region of the hippocampus could reflect synergistic effects between axonal loss and dysmyelination known to occur in WMI [49,117–119]. Previous studies using in vivo and *ex vivo* DTI of the hippocampus showed that increase in diffusivity, particularly in the CA1 region, could reflect pyramidal neurons death, dendritic loss and ongoing activation of glial cells

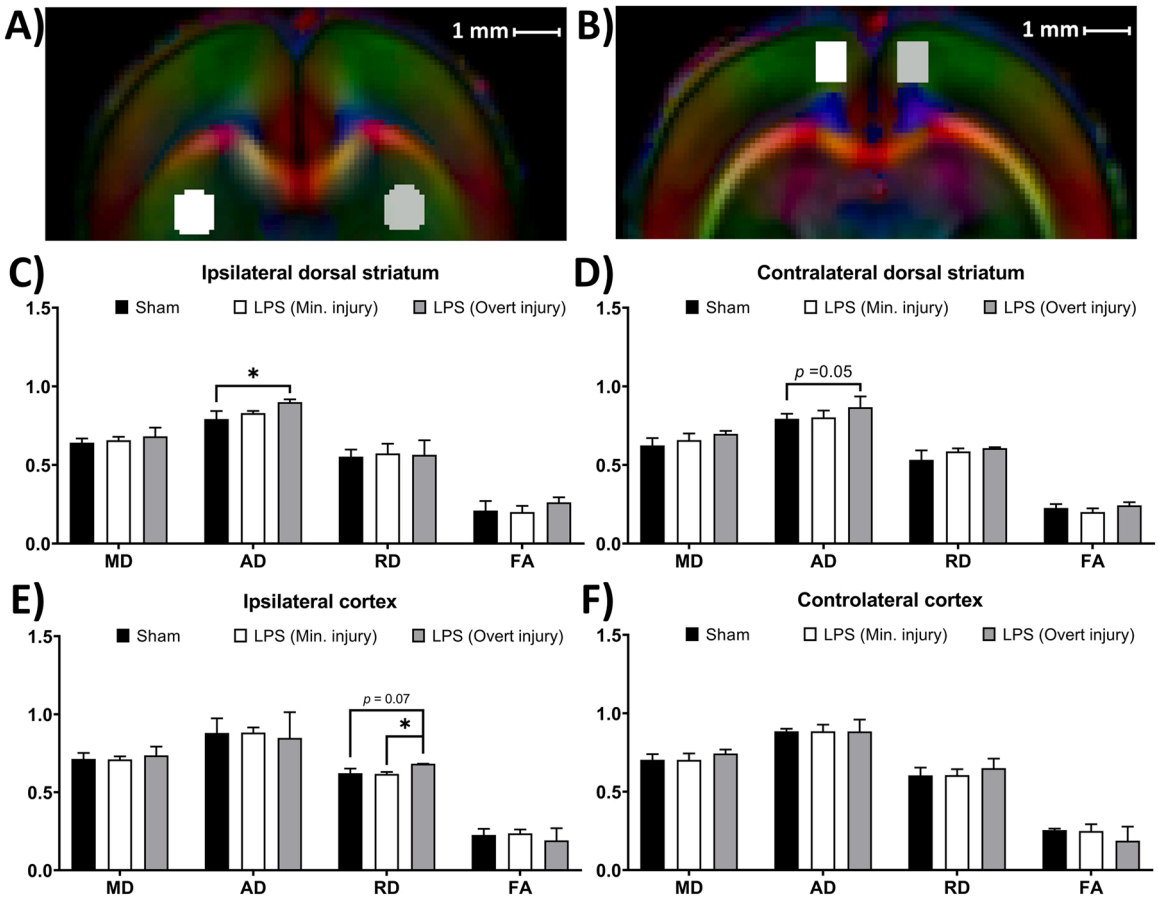

Fig. 6. *In vivo* diffusion tensor imaging of the dorsal striatum and cortex acquired at P31-P32 in rats exposed to neonatal LPS. Examples of coronal RGB (red, green, and blue) map with the highlighted ROIs for (A) the ipsilateral and contralateral striatum and (B) the ipsilateral and contralateral cortical region encompassing the motor and retrosplenial cortex. The ROI overlay depicts the ipsilateral side in white (left side) and the contralateral side in gray (right side). Bar graph of mean diffusivity (MD), axial diffusivity (AD), radial diffusivity (RD) and fractional anisotropy (FA) in (C) the ipsilateral dorsal striatum, (D) the contralateral dorsal striatum, and in the (E) the ipsilateral and (F) contralateral cortical region encompassing the motor and retrosplenial cortex. Values are represented as median ± 95% CI. * $p < 0.05$ compared to Sham or LPS (minimal injury). Diffusivity values (MD, AD and RD) are in: $\mu m^2 \cdot ms^{-1}$. (For interpretation of the references to colour in this figure legend, the reader is referred to the web version of this article.)

[120–123]. In this animal model of WMI, it has been demonstrated that hippocampal atrophy is accompanied by increased neuronal cell death and injury to axons and dendrites within the CA1 region [55,56]. Combined together, DTI assessed diffusivity changes in the fimbria and CA1 region that could reflect deleterious pathological processes due to hippocampal atrophy.

Additionally, we observed an increase in MD in the fimbria and CA1 region that was related to poorer performance during the fear conditioning test at P36–38. It is established that the hippocampus is crucial for memory formation particularly in the context of discrete cued fear conditioning paradigm such as the one used in this study [124–126]. In rodents, early life immune activation was associated to a disruption of hippocampus neurodevelopmental processes leading to learning and memory deficits [99,127–130]. Thus, the changes at DTI in the fimbria and CA1 region could result from deleterious pathological processes leading in the most severe cases to hippocampal atrophy (as seen on volumetric assessment) with subsequent Wallerian degeneration as previously published [131–133]. In summary, in vivo DTI is able to assess long-term microstructure changes in the white and gray matter within the hippocampal region that are associated to learning and memory impairments. To our knowledge, this is the first study to demonstrate that microstructural alterations at in vivo DTI in the hippocampal region were associated to learning and memory impairment using in neonatal LPS-induced WMI.

Analysis of diffusivity within the dorsal striatum, which encompasses the caudate nucleus and the putamen, revealed the presence of increased AD in animals with overt injury. This unexpected increase of AD in the striatum was also found in other human and animal studies [134,135]. As changes in AD are associated to neuronal integrity, the increase in AD could reflect axonal loss within the striatum [136]. Injury to the striatum, which includes macro- and microstructural alterations, has been consistently reported in VP-born individuals from term-equivalent age up to early adulthood [19,137–140]. Using the LPS-induced WMI model, it was demonstrated that LPS exposure led to increased apoptosis within the striatum during the acute phase of injury and was also associated with decreased striatum volume at adulthood [60,61]. Thus, the reported increase in AD could reflect neuron and axon loss possibly leading to striatum atrophy.

In the current study, we detected a trend toward increased radial diffusivity in the ipsilateral retrosplenial and motor cortical regions using in vivo DTI. Previously published data showed long-term alteration of cortical diffusivity parameters (MD, AD and RD) in preterm infants WMI and rodents' model of WMI [23,32,141,142]. Furthermore, increase in RD was associated to disruption of myelin integrity or long-lasting hypomyelination [136,143]. Within different cortical regions, perinatal LPS exposure led to neuronal alteration and hypomyelination in different animal species [53,144,145]. If confirmed, the changes in radial diffusivity seen with in vivo DTI could represent ongoing myelination alteration extending beyond the initial inflammatory insult.

Within the different ROIs analyzed at DTI, there was no significant alteration of FA except an increase in the contralateral CA2/CA3 region of the hippocampus. The lack of FA changes compared to MD, AD and RD is in accordance with several published studies in VP-born population. At term-equivalent age, MD, AD and RD changes had a more significance compared to FA in several types of white matter injury in VP-born infants [113,146,147]. Similarly, changes in FA were less significant compared to MD, AD and RD at long-term (up to adulthood) in VP-born individuals [148,149]. Thus, the lack of significant change in FA underlines the fact that changes in MD, AD and RD allow a better characterization of injury during the acute and chronic periods.

Qualitative analysis of MRI T2-weighted images at term equivalent age was used in clinical trials for the neuroprotective effect of erythropoietin on preterm infants [150–152]. Similarly, we evaluated the safety of hydrocortisone on the hippocampal integrity using basic structural MRI [12]. In this study, true FISP sequence allowed to acquire high-resolution T2-weighted images in a timely manner to assess volumetric changes in LPS-induced WMI neonatal model. True FISP sequence is known to produce high-quality images and is less susceptible to signal loss, motion artifacts and radiofrequency absorption [153,154], and was able to identify with accuracy macroscopic neuropathological consequences such as hippocampal atrophy as previously described in neonatal WMI models. Although, T2-weighted volumetric measurement did not correlate to behavioral deficits in our study, we believe that high resolution structural MRI with segmentation of pertinent regions remain highly relevant in the identification of neurodevelopmental disruptors or efficient neuroprotective strategies.

DTI was used as an imaging biomarker to assess white matter integrity at term equivalent age in clinical trials to assay the neuroprotective potential of melatonin, erythropoietin, and antenatal magnesium sulfate [155–158]. Knowing that multimodal MRI represent a promising non-invasive biomarker of cerebral integrity in clinical trials in preterm infants, there is currently a need for robust diffusion MRI (dMRI) method to acquire high resolution and high-quality images in a relatively short period of time. Within our study, DTI provided significant findings that related to outcome measures. Future diffusion imaging studies could consider the use of more advance methods to better confirm component changes in gray matter and white matter.

Multi-shell diffusion imaging methods, such as diffusion basis spectrum imaging (DBSI) would be an interesting choice [136]. The DBSI model allows the evaluation of intracellular diffusion, extracellular diffusion, water diffusion as well as diffusion of fiber groups [159–161]. More importantly, this method has been validated and is currently used to identify microstructural changes in patients suffering from multiple sclerosis [160,162]. Recently, researchers combined DBSI with machine learning algorithms as a new imaging biomarker to facilitate the detection and characterization of tumors in adult glioblastoma and pediatric high-grade brain tumors [163,164]. Thus, DBSI is an interesting model to further analyze component specific changes in our model of inflammation induced WMI.

Another multi-shell diffusion MRI technique is the neurite orientation dispersion and density imaging (NODDI) method. NODDI applied to datasets with only 3 or 4 b-values (including b =0) and assesses neurites density and the extent of neurites dispersion [165]. This method has been used to follow neurodevelopmental changes in preterm and term-born neonates [166–169]. During neurodevelopment, NODDI revealed an increase in orientation dispersion index within cortical gray matter that reached a plateau at 38 weeks post-menstrual age which was related to ongoing cortical neurite growth and dendritic arborization [166,168]. NODDI is an interesting method as it models accurately dendrite dispersion and density and is complementary to standard DTI measures.

One limitation of this study is that only male rats were used. Previous studies shown that there was no significant difference in extent of injury and neurobehavioral deficits between male and female rats exposed to intracerebral LPS during the neonatal period [49,56,170]. Thus, we believe that neonatal LPS exposure should led to similar insult in female rats. Nonetheless, this should be confirmed in future studies that include both sexes. The inclusion of male and female and analyses based on sex in preclinical studies will greatly improve current knowledge on sexually dimorphic differences particularly for the development of neuroprotective targets. Another limitation of this study is the lack of significant microstructural change between the LPS (Min. injury) and the Sham groups even in the presence of subtle behavioral changes at the fear conditioning. This shows the current limitation of the DTI technique in our study. The use of more advanced DTI techniques such as NODDI or DBSI, as discussed previously, open the possibility to detect subtle microstructural alterations in the animals showing minimal injury at MRI.

5. Conclusion

In conclusion, the present study demonstrated that in vivo multimodal MRI techniques (volumetric and DTI) allow a thorough evaluation of extent of brain injury following neonatal LPS-induced WMI. Animals more severely affected presented ventriculomegaly and hippocampal atrophy on T2-weighted images and alteration at DTI in the striatum and the cortex. Furthermore, microstructural changes at DTI in the hippocampal formation (particularly in the fimbria and the CA1 region) were related to learning and memory impairments in our animal model. The results presented in this study further consolidate the potency of DTI as a robust marker of ongoing neurodevelopmental alterations following injuries in the immature brain. As multimodal MRI is becoming more readily available and used in the neonatal intensive care unit, it is becoming essential to understand its full potency as a robust and sensitive tool for early evaluation and follow-up of neuroprotective response in the development of future therapeutic targets.

CRediT authorship contribution statement

Wyston Pierre participated in data acquisition, data analysis, and manuscript draft, reviewed, and revised the manuscript. Erjun Zhang contributed to data analysis and manuscript draft. Irène Londono contributed to the study preparation, data acquisition and manuscript preparation. Benjamin De Leener and Frédéric Lesage have revised the manuscript. Gregory Anton Lodygensky conceptualized and designed the study, contributed to data acquisition, supervised the data analysis, and revised the manuscript.

Acknowledgment

This work was supported by grants from the Canadian Institutes of Health Research (http://www.cihr-irsc.gc.ca/) – Institute of Human Development, Child and Youth Health (IHDCYH), Canada (Grant #136908 to G.A.L.). G.A.L. is supported by a start-up grant from the Research Center of CHU Sainte-Justine and the Fonds de recherche du Québec – Santé (FRQS). B.D.L. is supported by Polytechnique Montreal and by the TransMedTech Institute Chair in Pediatric Neuroimaging. We would like to thank Philippe Pouliot for his help with the in vivo MRI acquisition.

Conflict of interest

The authors declare no competing financial interests.

Appendix A. Supporting information

Supplementary data associated with this article can be found in the online version at doi:10.1016/j.bbr.2022.113884.

References

[1] E.F. Maalouf, P.J. Duggan, S.J. Counsell, M.A. Rutherford, F. Cowan, D. Azzopardi, A.D. Edwards, Comparison of findings on cranial ultrasound and magnetic resonance imaging in preterm infants, Pediatrics 107 (4) (2001) 719–727.

[2] G.A. Lodygensky, D.K. Thompson, Toward quantitative MRI analysis, Neurology 88 (7) (2017) 610–611.

[3] O. Khwaja, J.J. Volpe, Pathogenesis of cerebral white matter injury of prematurity, Arch. Dis. Child. Fetal Neonatal Ed. 93 (2) (2008) F153–F161.

[4] J.J. Volpe, Brain injury in premature infants: a complex amalgam of destructive and developmental disturbances, Lancet Neurol. 8 (1) (2009) 110–124.

[5] J.J. Neil, J.J. Volpe, Chapter 16 - encephalopathy of prematurity: clinical-neurological features, diagnosis, imaging, prognosis, therapy, in: J.J. Volpe, T. E. Inder, B.T. Darras, L.S. de Vries, A.J. du Plessis, J.J. Neil, J.M. Perlman (Eds.), Volpe's Neurology of the Newborn (Sixth Edition), Elsevier, 2018, pp. 425–457. e11.

[6] C. Jin, I. Londono, C. Mallard, G.A. Lodygensky, New means to assess neonatal inflammatory brain injury, J. Neuroinflamm. 12 (1) (2015) 180.

[7] V. Enguix, Y. Ding, G.A. Lodygensky, Recent advances in preclinical and clinical multimodal MR in the newborn brain, J. Magn. Reson. 292 (2018) 149–154.

[8] D.K. Thompson, L.G. Matthews, B. Alexander, K.J. Lee, C.E. Kelly, C.L. Adamson, R.W. Hunt, J.L.Y. Cheong, M. Spencer-Smith, J.J. Neil, M.L. Seal, T.E. Inder, L. W. Doyle, P.J. Anderson, Tracking regional brain growth up to age 13 in children born term and very preterm, Nat. Commun. 11 (1) (2020) 696.

[9] K. Keunen, K.J. Kersbergen, F. Groenendaal, I. Isgum, L.S. de Vries, M.J. Benders, Brain tissue volumes in preterm infants: prematurity, perinatal risk factors and neurodevelopmental outcome: a systematic review, J. Matern. Fetal Neonatal Med. 25 (1) (2012) 89–100.

[10] K. Keunen, I. Išgum, B.J.M. van Kooij, P. Anbeek, I.C. van Haastert, C. Koopman-Esseboom, P.C. Fieret-van Stam, R.A.J. Nievelstein, M.A. Viergever, L.S. de Vries, F. Groenendaal, M.J.N.L. Benders, Brain volumes at term-equivalent age in preterm infants: imaging biomarkers for neurodevelopmental outcome through early school age, J. Pedia 172 (2016) 88–95.

[11] H. El Marroun, R. Zou, M.F. Leeuwenburg, E.A.P. Steegers, I.K.M. Reiss, R. L. Muetzel, S.A. Kushner, H. Tiemeier, Association of gestational age at birth with brain morphometry, JAMA Pedia 174 (12) (2020) 1149–1158.

[12] G.A. Lodygensky, K. Rademaker, S. Zimine, M. Gex-Fabry, A.F. Lieftink, F. Lazeyras, F. Groenendaal, L.S. de Vries, P.S. Huppi, Structural and functional brain development after hydrocortisone treatment for neonatal chronic lung disease, Pediatrics 116 (1) (2005) 1–7.

[13] D.K. Thompson, S.J. Wood, L.W. Doyle, S.K. Warfield, G.A. Lodygensky, P. J. Anderson, G.F. Egan, T.E. Inder, Neonate hippocampal volumes: prematurity, perinatal predictors, and 2-year outcome, Ann. Neurol. 63 (5) (2008) 642–651.

[14] C. Omizzolo, D.K. Thompson, S.E. Scratch, R. Stargatt, K.J. Lee, J. Cheong, G. Roberts, L.W. Doyle, P.J. Anderson, Hippocampal volume and memory and learning outcomes at 7 years in children born very preterm, J. Int. Neuropsychol. Soc.: JINS 19 (10) (2013) 1065–1075.

[15] D.K. Thompson, C. Omizzolo, C. Adamson, K.J. Lee, R. Stargatt, G.F. Egan, L. W. Doyle, T.E. Inder, P.J. Anderson, Longitudinal growth and morphology of the hippocampus through childhood: Impact of prematurity and implications for memory and learning, Hum. Brain Mapp. 35 (8) (2014) 4129–4139.

[16] S. Aanes, K.J. Bjuland, J. Skranes, G.C.C. Løhaugen, Memory function and hippocampal volumes in preterm born very-low-birth-weight (VLBW) young adults, Neuroimage 105 (2015) 76–83.

[17] M.H. Beauchamp, D.K. Thompson, K. Howard, L.W. Doyle, G.F. Egan, T.E. Inder, P.J. Anderson, Preterm infant hippocampal volumes correlate with later working memory deficits, Brain 131 (Pt 11) (2008) 2986–2994.

[18] C. Nosarti, S. Froudist-Walsh, Alterations in development of hippocampal and cortical memory mechanisms following very preterm birth, Dev. Med. Child Neurol. 58 (S4) (2016) 35–45.

[19] C. Nosarti, K.W. Nam, M. Walshe, R.M. Murray, M. Cuddy, L. Rifkin, M.P.G. Allin, Preterm birth and structural brain alterations in early adulthood, NeuroImage: Clin. 6 (2014) 180–191.

[20] S.J. Counsell, M.A. Rutherford, F.M. Cowan, A.D. Edwards, Magnetic resonance imaging of preterm brain injury, Arch. Dis. Child. - Fetal Neonatal Ed. 88 (4) (2003) F269–F274.

[21] J.J. Neil, S.I. Shiran, R.C. McKinstry, G.L. Schefft, A.Z. Snyder, C.R. Almli, E. Akbudak, J.A. Aronovitz, J.P. Miller, B.C. Lee, T.E. Conturo, Normal brain in human newborns: apparent diffusion coefficient and diffusion anisotropy measured by using diffusion tensor MR imaging, Radiology 209 (1) (1998) 57–66.

[22] J.J. Neil, C.D. Smyser, Recent advances in the use of MRI to assess early human cortical development, J. Magn. Reson. 293 (2018) 56–69.

[23] T.A. Smyser, C.D. Smyser, C.E. Rogers, S.K. Gillespie, T.E. Inder, J.J. Neil, Cortical gray and adjacent white matter demonstrate synchronous maturation in very preterm infants, Cereb. Cortex 26 (8) (2016) 3370–3378.

[24] R.E. Lean, R.H. Han, T.A. Smyser, J.K. Kenley, J.S. Shimony, C.E. Rogers, D. D. Limbrick Jr., C.D. Smyser, Altered neonatal white and gray matter microstructure is associated with neurodevelopmental impairments in very preterm infants with high-grade brain injury, Pediatr. Res. 86 (3) (2019) 365–374.

[25] L. Eikenes, G.C. Løhaugen, A.M. Brubakk, J. Skranes, A.K. Håberg, Young adults born preterm with very low birth weight demonstrate widespread white matter alterations on brain DTI, Neuroimage 54 (3) (2011) 1774–1785.

[26] S.J. Short, J.T. Elison, B.D. Goldman, M. Styner, H. Gu, M. Connelly, E. Maltbie, S. Woolson, W. Lin, G. Gerig, J.S. Reznick, J.H. Gilmore, Associations between white matter microstructure and infants' working memory, Neuroimage 64 (2013) 156–166.

[27] D.K. Thompson, K.J. Lee, G.F. Egan, S.K. Warfield, L.W. Doyle, P.J. Anderson, T. E. Inder, Regional white matter microstructure in very preterm infants: predictors and 7 year outcomes, Cortex 52 (2014) 60–74.

[28] J.M. Young, B.R. Morgan, H.E.A. Whyte, W. Lee, M.L. Smith, C. Raybaud, M. M. Shroff, J.G. Sled, M.J. Taylor, Longitudinal study of white matter development and outcomes in children born very preterm, Cereb. Cortex 27 (8) (2016) 4094–4105.

[29] I.M.H. Hollund, A. Olsen, J. Skranes, A.-M. Brubakk, A.K. Håberg, L. Eikenes, K.A. I. Evensen, White matter alterations and their associations with motor function in young adults born preterm with very low birth weight, NeuroImage. Clin. 17 (2017) 241–250.

[30] A.M. Mathur, J.J. Neil, T.E. Inder, Understanding brain injury and neurodevelopmental disabilities in the preterm infant: the evolving role of advanced magnetic resonance imaging, Semin. Perinatol. 34 (1) (2010) 57–66.

[31] J. Lubsen, B. Vohr, E. Myers, M. Hampson, C. Lacadie, K.C. Schneider, K.H. Katz, R.T. Constable, L.R. Ment, Microstructural and functional connectivity in the developing preterm brain, Semin. Perinatol. 35 (1) (2011) 34–43.

[32] G. Ball, L. Srinivasan, P. Aljabar, S.J. Counsell, G. Durighel, J.V. Hajnal, M. A. Rutherford, A.D. Edwards, Development of cortical microstructure in the preterm human brain, Proc. Natl. Acad. Sci. U.S.A. 110 (23) (2013) 9541–9546.

[33] R.C. McKinstry, J.H. Miller, A.Z. Snyder, A. Mathur, G.L. Schefft, C.R. Almli, J. S. Shimony, S.I. Shiran, J.J. Neil, A prospective, longitudinal diffusion tensor imaging study of brain injury in newborns, Neurology 59 (6) (2002) 824–833.

[34] B.B. Monson, Z. Eaton-Rosen, K. Kapur, E. Liebenthal, A. Brownell, C.D. Smyser, C.E. Rogers, T.E. Inder, S.K. Warfield, J.J. Neil, Differential rates of perinatal maturation of human primary and nonprimary auditory cortex, ENEURO.0380-17.2017, eNeuro 5 (1) (2018).

[35] J. Uh, T.E. Merchant, H.M. Conklin, Y. Ismael, Y. Li, Y. Han, N.D. Sabin, A. Babajani-Feremi, D.J. Indelicato, C.H. Hua, Diffusion tensor imaging-based analysis of baseline neurocognitive function and posttreatment white matter changes in pediatric patients with craniopharyngioma treated with surgery and proton therapy, Int. J. Radiat. Oncol. Biol. Phys. 109 (2) (2021) 515–526.

[36] T. Sun, Y. Xu, C. Pan, Y. Liu, Y. Tian, C. Li, F. Di, L. Zhang, Surgical treatment and prognosis of focal brainstem gliomas in children: a 7 year single center experience, Medicine 99 (36) (2020), e22029.

[37] A. Vedantam, K.M. Stormes, N. Gadgil, S.F. Kralik, G. Aldave, S.K. Lam, Association between postoperative DTI metrics and neurological deficits after posterior fossa tumor resection in children, J. Neurosurg. Pedia 24 (2019) 1–7.

[38] R.M. Polan, A. Poretti, T.A. Huisman, T. Bosemani, Susceptibility-weighted imaging in pediatric arterial ischemic stroke: a valuable alternative for the noninvasive evaluation of altered cerebral hemodynamics, AJNR Am. J. Neuroradiol. 36 (4) (2015) 783–788.

[39] B.P. Jones, V. Ganesan, D.E. Saunders, W.K. Chong, Imaging in childhood arterial ischaemic stroke, Neuroradiology 52 (6) (2010) 577–589.

[40] R.J. Seitz, G.A. Donnan, Role of neuroimaging in promoting long-term recovery from ischemic stroke, J. Magn. Reson. Imaging 32 (4) (2010) 756–772.

[41] D. Pinter, T. Gattringer, S. Fandler-Höfler, M. Kneihsl, S. Eppinger, H. Deutschmann, A. Pichler, B. Poltrum, G. Reishofer, S. Ropele, R. Schmidt, C. Enzinger, Early progressive changes in white matter integrity are associated with stroke recovery, Transl. Stroke Res. 11 (6) (2020) 1264–1272.

[42] L. Xue, C. Pei, X. Wang, H. Wang, S. Tian, Z. Yao, Q. Lu, Predicting neuroimaging biomarkers for antidepressant selection in early treatment of depression, J. Magn. Reson. Imaging 54 (2) (2021) 551–559.

[43] X. He, E. Pueraro, Y. Kim, C.M. Garcia, B. Maas, J. Choi, D.A. Egglefield, S. Schiff, J.R. Sneed, P.J. Brown, A.M. Brickman, S.P. Roose, B.R. Rutherford, Association of white matter integrity with executive function and antidepressant treatment outcome in patients with late-life depression, Am. J. Geriatr. Psychiatry 29 (2021) 1188–1198.

[44] E.M.T. Melloni, S. Poletti, S. Dallaspezia, I. Bollettini, B. Vai, B. Barbini, R. Zanardi, C. Colombo, F. Benedetti, Changes of white matter microstructure after successful treatment of bipolar depression, J. Affect. Disord. 274 (2020) 1049–1056.

[45] V. Ginet, Y. van de Looij, V. Petrenko, A. Toulotte, J. Kiss, P.S. Huppi, S. V. Sizonenko, Lactoferrin during lactation reduces lipopolysaccharide-induced brain injury, Biofactors 42 (3) (2016) 323–336.

[46] Y. van de Looij, V. Ginet, A. Chatagner, A. Toulotte, E. Somm, P.S. Huppi, S. V. Sizonenko, Lactoferrin during lactation protects the immature hypoxic-ischemic rat brain, Ann. Clin. Transl. Neurol. 1 (12) (2014) 955–967.

[47] Y. van de Looij, A. Chatagner, C. Quairiaux, R. Gruetter, P.S. Huppi, S. V. Sizonenko, Multi-modal assessment of long-term erythropoietin treatment after neonatal hypoxic-ischemic injury in rat brain, PLoS One 9 (4) (2014), e95643.

[48] W.C. Pierre, L. Akakpo, I. Londono, P. Pouliot, S. Chemtob, F. Lesage, G. A. Lodygensky, Assessing therapeutic response non-invasively in a neonatal rat model of acute inflammatory white matter injury using high-field MRI, Brain. Behav. Immun. 81 (2019) 348–360.

[49] Y. Pang, Z. Cai, P.G. Rhodes, Disturbance of oligodendrocyte development, hypomyelination and white matter injury in the neonatal rat brain after intracerebral injection of lipopolysaccharide, Brain Res. Dev. 140 (2) (2003) 205–214.

[50] Z. Cai, Y. Pang, S. Lin, P.G. Rhodes, Differential roles of tumor necrosis factor-alpha and interleukin-1 beta in lipopolysaccharide-induced brain injury in the neonatal rat, Brain Res. 975 (1–2) (2003) 37–47.

[51] B.D. Semple, K. Blomgren, K. Gimlin, D.M. Ferriero, L.J. Noble-Haeusslein, Brain development in rodents and humans: Identifying benchmarks of maturation and vulnerability to injury across species, Prog. Neurobiol. 0 (2013) 1–16.
[52] L. Akakpo, W.C. Pierre, C. Jin, I. Londono, P. Pouliot, G.A. Lodygensky, User-independent diffusion tensor imaging analysis pipelines in a rat model presenting ventriculomegalia: a comparison study, NMR Biomed. 30 (11) (2017), e3793.
[53] E.P. Demina, W.C. Pierre, A.L.A. Nguyen, I. Londono, B. Reiz, C. Zou, R. Chakraberty, C.W. Cairo, A.V. Pshezhetsky, G.A. Lodygensky, Persistent reduction in sialylation of cerebral glycoproteins following postnatal inflammatory exposure, J. Neuroinflamm. 15 (1) (2018) 336.
[54] W.C. Pierre, L.M. Legault, I. Londono, S. McGraw, G.A. Lodygensky, Alteration of the brain methylation landscape following postnatal inflammatory injury in rat pups, FASEB J. 34 (1) (2020) 432–445.
[55] L.W. Fan, Y. Pang, S. Lin, L.T. Tien, T. Ma, P.G. Rhodes, Z. Cai, Minocycline reduces lipopolysaccharide-induced neurological dysfunction and brain injury in the neonatal rat, J. Neurosci. Res. 82 (1) (2005) 71–82.
[56] L.W. Fan, L.T. Tien, H.J. Mitchell, P.G. Rhodes, Z. Cai, Alpha-phenyl-n-tert-butyl-nitrone ameliorates hippocampal injury and improves learning and memory in juvenile rats following neonatal exposure to lipopolysaccharide, Eur. J. Neurosci. 27 (6) (2008) 1475–1484.
[57] L.W. Fan, H.J. Mitchell, P.G. Rhodes, Z. Cai, Alpha-Phenyl-n-tert-butyl-nitrone attenuates lipopolysaccharide-induced neuronal injury in the neonatal rat brain, Neuroscience 151 (3) (2008) 737–744.
[58] L.W. Fan, L.T. Tien, B. Zheng, Y. Pang, R.C. Lin, K.L. Simpson, T. Ma, P.G. Rhodes, Z. Cai, Dopaminergic neuronal injury in the adult rat brain following neonatal exposure to lipopolysaccharide and the silent neurotoxicity, Brain. Behav. Immun. 25 (2) (2011) 286–297.
[59] Y. Pang, L.W. Fan, B. Zheng, L.R. Campbell, Z. Cai, P.G. Rhodes, Dexamethasone and betamethasone protect against lipopolysaccharide-induced brain damage in neonatal rats, Pediatr. Res. 71 (5) (2012) 552–558.
[60] K.C. Wang, L.W. Fan, A. Kaizaki, Y. Pang, Z. Cai, L.T. Tien, Neonatal lipopolysaccharide exposure induces long-lasting learning impairment, less anxiety-like response and hippocampal injury in adult rats, Neuroscience 234 (2013) 146–157.
[61] G.A. Lodygensky, N. Kunz, E. Perroud, E. Somm, V. Mlynarik, P.S. Huppi, R. Gruetter, S.V. Sizonenko, Definition and quantification of acute inflammatory white matter injury in the immature brain by MRI/MRS at high magnetic field, Pediatr. Res. 75 (3) (2014) 415–423.
[62] G.A. Lodygensky, T. West, M. Stump, D.M. Holtzman, T.E. Inder, J.J. Neil, In vivo MRI analysis of an inflammatory injury in the developing brain, Brain. Behav. Immun. 24 (5) (2010) 759–767.
[63] R. Ramachandra, T. Subramanian, Atlas of the Neonatal Rat Brain, CRC Press, Boca Raton, FL, 2011.
[64] A. Castonguay, J. Lefebvre, F. Lesage, P. Pouliot, Comparing three-dimensional serial optical coherence tomography histology to MRI imaging in the entire mouse brain, J. Biomed. Opt. 23 (1) (2018) 1–9.
[65] B.D. Semple, J. Carlson, L.J. Noble-Haeusslein, Pediatric Rodent Models of Traumatic Brain Injury, Methods Mol. Biol. 1462 (2016) 325–343.
[66] P. Delafontaine-Martel, J. Lefebvre, P.L. Tardif, B.I. Lévy, P. Pouliot, F. Lesage, Whole brain vascular imaging in a mouse model of Alzheimer's disease with two-photon microscopy, J. Biomed. Opt. 23 (7) (2018) 1–10.
[67] J. Schindelin, I. Arganda-Carreras, E. Frise, V. Kaynig, M. Longair, T. Pietzsch, S. Preibisch, C. Rueden, S. Saalfeld, B. Schmid, J.-Y. Tinevez, D.J. White, V. Hartenstein, K. Eliceiri, P. Tomancak, A. Cardona, Fiji: an open-source platform for biological-image analysis, Nat. Methods 9 (7) (2012) 676–682.
[68] L.C. Chang, D.K. Jones, C. Pierpaoli, RESTORE: robust estimation of tensors by outlier rejection, Magn. Reson. Med. 53 (5) (2005) 1088–1095.
[69] E. Garyfallidis, M. Brett, B. Amirbekian, A. Rokem, S. van der Walt, M. Descoteaux, I. Nimmo-Smith, Dipy, a library for the analysis of diffusion MRI data, Front. Neuroinform. 8 (2014) 8.
[70] H. Zhang, P.A. Yushkevich, D.C. Alexander, J.C. Gee, Deformable registration of diffusion tensor MR images with explicit orientation optimization, Med. Image Anal. 10 (5) (2006) 764–785.
[71] A. Rumple, M. McMurray, J. Johns, J. Lauder, P. Makam, M. Radcliffe, I. Oguz, 3-dimensional diffusion tensor imaging (DTI) atlas of the rat brain, PLoS One 8 (7) (2013), e67334.
[72] A. Narberhaus, D. Segarra, X. Caldú, M. Giménez, R. Pueyo, F. Botet, C. Junqué, Corpus callosum and prefrontal functions in adolescents with history of very preterm birth, Neuropsychologia 46 (1) (2008) 111–116.
[73] A. Narberhaus, D. Segarra, X. Caldú, M. Giménez, C. Junqué, R. Pueyo, F. Botet, Gestational age at preterm birth in relation to corpus callosum and general cognitive outcome in adolescents, J. Child Neurol. 22 (6) (2007) 761–765.
[74] K.H.T. Cho, M. Fraser, B. Xu, J.M. Dean, A.J. Gunn, L. Bennet, Induction of tertiary phase epileptiform discharges after postasphyxial infusion of a toll-like receptor 7 agonist in preterm fetal sheep, Int. J. Mol. Sci. 22 (12) (2021) 6593.
[75] E. McClendon, K. Wang, K. Degener-O'Brien, M.W. Hagen, X. Gong, T. Nguyen, W.W. Wu, J. Maylie, S.A. Back, Transient hypoxemia disrupts anatomical and functional maturation of preterm fetal ovine CA1 pyramidal neurons, J. Neurosci. 39 (40) (2019) 7853–7871.
[76] T. Bartsch, J. Döhring, S. Reuter, C. Finke, A. Rohr, H. Brauer, G. Deuschl, O. Jansen, Selective neuronal vulnerability of human hippocampal CA1 neurons: lesion evolution, temporal course, and pattern of hippocampal damage in diffusion-weighted MR imaging, J. Cereb. Blood Flow. Metab. 35 (11) (2015) 1836–1845.
[77] J.H. Cole, M.L. Filippetti, M.P. Allin, M. Walshe, K.W. Nam, B.A. Gutman, R. M. Murray, L. Rifkin, P.M. Thompson, C. Nosarti, Subregional Hippocampal Morphology and Psychiatric Outcome in Adolescents Who Were Born Very Preterm and at Term, PLoS ONE 10 (6) (2015), e0130094.
[78] E. Guevara, W.C. Pierre, C. Tessier, L. Akakpo, I. Londono, F. Lesage, G. A. Lodygensky, Altered Functional Connectivity Following an Inflammatory White Matter Injury in the Newborn Rat: A High Spatial and Temporal Resolution Intrinsic Optical Imaging Study, Front Neurosci. 11 (2017) 358.
[79] S.M. Smith, M. Jenkinson, M.W. Woolrich, C.F. Beckmann, T.E. Behrens, H. Johansen-Berg, P.R. Bannister, M. De Luca, I. Drobnjak, D.E. Flitney, R. K. Niazy, J. Saunders, J. Vickers, Y. Zhang, N. De Stefano, J.M. Brady, P. M. Matthews, Advances in functional and structural MR image analysis and implementation as FSL, Neuroimage 23 (1) (2004) S208–S219.
[80] A.L. Deal, K.J. Erickson, S.I. Shiers, M.A. Burman, Limbic system development underlies the emergence of classical fear conditioning during the third and fourth weeks of life in the rat, Behav. Neurosci. 130 (2) (2016) 212–230.
[81] M.S. Fanselow, From contextual fear to a dynamic view of memory systems, Trends Cogn. Sci. 14 (1) (2010) 7–15.
[82] N.T. Sanon, J. Gagné, D.C. Wolf, S. Aboulamer, C.M. Bosoi, A. Simard, E. Messiet, S. Desgent, L. Carmant, Favorable adverse effect profile of brivaracetam vs levetiracetam in a preclinical model, Epilepsy Behav. 79 (2018) 117–125.
[83] J. Erlich, D. Bush, J. LeDoux, The role of the lateral amygdala in the retrieval and maintenance of fear-memories formed by repeated probabilistic reinforcement, Front. Behav. Neurosci. 6 (16) (2012).
[84] M.R. Gilmartin, N.L. Balderston, F.J. Helmstetter, Prefrontal cortical regulation of fear learning, Trends Neurosci. 37 (8) (2014) 455–464.
[85] H. Elahi, V. Hong, J.E. Ploski, Electroconvulsive shock does not impair the reconsolidation of cued and contextual pavlovian threat memory, Int. J. Mol. Sci. 21 (19) (2020) 7072.
[86] M.E. Hopkins, D.J. Bucci, Interpreting the effects of exercise on fear conditioning: The influence of time of day, Behav. Neurosci. 124 (6) (2010) 868–872.
[87] M.A. Burman, C.A. Simmons, M. Hughes, L. Lei, Developing and validating trace fear conditioning protocols in C57BL/6 mice, J. Neurosci. Methods 222 (2014) 111–117.
[88] N. Chaaya, A. Jacques, A. Belmer, K. Beecher, S.A. Ali, F. Chehrehasa, A.R. Battle, L.R. Johnson, S.E. Bartlett, Contextual fear conditioning alter microglia number and morphology in the rat dorsal hippocampus, Front. Cell. Neurosci. 13 (214) (2019) 214.
[89] N. Schroyens, C.L. Bender, J.M. Alfei, V.A. Molina, L. Luyten, T. Beckers, Post-weaning housing conditions influence freezing during contextual fear conditioning in adult rats, Behav. Brain Res. 359 (2019) 172–180.
[90] N. Chaaya, J. Wang, A. Jacques, K. Beecher, M. Chaaya, A.R. Battle, L.R. Johnson, F. Chehrehasa, A. Belmer, S.E. Bartlett, Contextual fear memory maintenance changes expression of pMAPK, BDNF and IBA-1 in the pre-limbic cortex in a layer-specific manner, Front. Neural Circuits 15 (61) (2021), 660199.
[91] J. Freund, A.M. Brandmaier, L. Lewejohann, I. Kirste, M. Kritzler, A. Krüger, N. Sachser, U. Lindenberger, G. Kempermann, Emergence of individuality in genetically identical mice, Science 340 (6133) (2013) 756–759.
[92] M.H. van der Goot, M. Kooij, S. Stolte, A. Baars, S.S. Arndt, H.A. van Lith, Incorporating inter-individual variability in experimental design improves the quality of results of animal experiments, PLoS One 16 (8) (2021), e0255521.
[93] B. Voelkl, N.S. Altman, A. Forsman, W. Forstmeier, J. Gurevitch, I. Jaric, N. A. Karp, M.J. Kas, H. Schielzeth, T. Van de Casteele, H. Würbel, Reproducibility of animal research in light of biological variation, Nat. Rev. Neurosci. 21 (7) (2020) 384–393.
[94] T.R. Wood, J.K. Gundersen, M. Falck, E. Maes, D. Osredkar, E.M. Løberg, H. Sabir, L. Walløe, M. Thoresen, Variability and sex-dependence of hypothermic neuroprotection in a rat model of neonatal hypoxic–ischaemic brain injury: a single laboratory meta-analysis, Sci. Rep. 10 (1) (2020) 10833.
[95] E. Manninen, K. Chary, N. Lapinlampi, P. Andrade, T. Paananen, A. Sierra, J. Tohka, O. Gröhn, A. Pitkänen, Early increase in cortical T2 relaxation is a prognostic biomarker for the evolution of severe cortical damage, but not for epileptogenesis, after experimental traumatic brain injury, J. Neurotrauma 37 (23) (2020) 2580–2594.
[96] Y. Wang, P. Andrade, A. Pitkänen, Peripheral infection after traumatic brain injury augments excitability in the perilesional cortex and dentate gyrus, Biomedicines 9 (12) (2021) 1946.
[97] K. Sherman, V. Woyach, J.C. Eisenach, F.A. Hopp, F. Cao, Q.H. Hogan, C. Dean, Heterogeneity in patterns of pain development after nerve injury in rats and the influence of sex, Neurobiol. Pain. 10 (2021), 100069.
[98] D. Dai, Y. Gao, J. Chen, Y. Huang, Z. Zhang, F. Xu, Time-resolved metabolomics analysis of individual differences during the early stage of lipopolysaccharide-treated rats, Sci. Rep. 6 (1) (2016) 34136.
[99] R.A. Kohman, A.J. Tarr, N.L. Sparkman, T.M. Bogale, G.W. Boehm, Neonatal endotoxin exposure impairs avoidance learning and attenuates endotoxin-induced sickness behavior and central IL-1beta gene transcription in adulthood, Behav. Brain Res. 194 (1) (2008) 25–31.
[100] K.M. Lan, L.T. Tien, Y. Pang, A.J. Bhatt, L.W. Fan, IL-1 receptor antagonist attenuates neonatal lipopolysaccharide-induced long-lasting learning impairment and hippocampal injury in adult rats, Toxicol. Lett. 234 (1) (2015) 30–39.
[101] H.C. Bergstrom, The neurocircuitry of remote cued fear memory, Neurosci. Biobehav. Rev. 71 (2016) 409–417.
[102] T.F. Giustino, S. Maren, The Role of the Medial Prefrontal Cortex in the Conditioning and Extinction of Fear, Front. Behav. Neurosci. 9 (298) (2015).
[103] T.P. Todd, D.I. Fournier, D.J. Bucci, Retrosplenial cortex and its role in cue-specific learning and memory, Neurosci. Biobehav. Rev. 107 (2019) 713–728.
[104] S.A. Back, P.A. Rosenberg, Pathophysiology of glia in perinatal white matter injury, Glia 62 (2014) 1790–1815.

[105] L.R. Campbell, Y. Pang, N.B. Ojeda, B. Zheng, P.G. Rhodes, B.T. Alexander, Intracerebral lipopolysaccharide induces neuroinflammatory change and augmented brain injury in growth-restricted neonatal rats, Pediatr. Res. 71 (6) (2012) 645–652.
[106] R.A. Dorner, V.J. Burton, M.C. Allen, S. Robinson, B.P. Soares, Preterm neuroimaging and neurodevelopmental outcome: a focus on intraventricular hemorrhage, post-hemorrhagic hydrocephalus, and associated brain injury, J. Perinatol.: Off. J. Calif. Perinat. Assoc. 38 (11) (2018) 1431–1443.
[107] A. Leviton, F. Gilles, Ventriculomegaly, delayed myelination, white matter hypoplasia, and "periventricular" leukomalacia: how are they related? Pediatr. Neurol. 15 (2) (1996) 127–136.
[108] A.M. Isaacs, C.D. Smyser, R.E. Lean, D. Alexopoulos, R.H. Han, J.J. Neil, S. A. Zimbalist, C.E. Rogers, Y. Yan, J.S. Shimony, D.D. Limbrick Jr., MR diffusion changes in the perimeter of the lateral ventricles demonstrate periventricular injury in post-hemorrhagic hydrocephalus of prematurity, Neuroimage Clin. 24 (2019), 102031.
[109] D.M. Hedderich, T. Boeckh-Behrens, J.G. Bäuml, A. Menegaux, M. Daamen, C. Zimmer, P. Bartmann, L. Scheef, H. Boecker, D. Wolke, C. Sorg, J.E. Spiro, Sequelae of Premature Birth in Young Adults: Incidental Findings on Routine Brain MRI, Clin. Neuroradiol. 31 (2) (2021) 325–333.
[110] Y. Pang, B. Zheng, L.R. Campbell, L.W. Fan, Z. Cai, P.G. Rhodes, IGF-1 can either protect against or increase LPS-induced damage in the developing rat brain, Pediatr. Res. 67 (6) (2010) 579–584.
[111] J.M. Strahle, R.L. Triplett, D. Alexopoulos, T.A. Smyser, C.E. Rogers, D. D. Limbrick, C.D. Smyser, Impaired hippocampal development and outcomes in very preterm infants with perinatal brain injury, NeuroImage: Clin. 22 (2019), 101787.
[112] D.K. Thompson, C. Adamson, G. Roberts, N. Faggian, S.J. Wood, S.K. Warfield, L. W. Doyle, P.J. Anderson, G.F. Egan, T.E. Inder, Hippocampal shape variations at term equivalent age in very preterm infants compared with term controls: perinatal predictors and functional significance at age 7, Neuroimage 70 (2013) 278–287.
[113] D.K. Thompson, T.E. Inder, N. Faggian, L. Johnston, S.K. Warfield, P.J. Anderson, L.W. Doyle, G.F. Egan, Characterization of the corpus callosum in very preterm and full-term infants utilizing MRI, Neuroimage 55 (2) (2011) 479–490.
[114] M.L. Krishnan, L.E. Dyet, J.P. Boardman, O. Kapellou, J.M. Allsop, F. Cowan, A. D. Edwards, M.A. Rutherford, S.J. Counsell, Relationship between white matter apparent diffusion coefficients in preterm infants at term-equivalent age and developmental outcome at 2 years, Pediatrics 120 (3) (2007) e604–e609.
[115] A.C. Nagasunder, H.C. Kinney, S. Blüml, C.J. Tavaré, T. Rosser, F.H. Gilles, M. D. Nelson, A. Panigrahy, Abnormal microstructure of the atrophic thalamus in preterm survivors with periventricular leukomalacia, Am. J. Neuroradiol. 32 (1) (2011) 185–191.
[116] D.K. Thompson, C.E. Kelly, J. Chen, R. Beare, B. Alexander, M.L. Seal, K.J. Lee, L. G. Matthews, P.J. Anderson, L.W. Doyle, J.L.Y. Cheong, A.J. Spittle, Characterisation of brain volume and microstructure at term-equivalent age in infants born across the gestational age spectrum, NeuroImage: Clin. 21 (2019), 101630.
[117] W. Pietrasik, I. Cribben, F. Olsen, Y. Huang, N.V. Malykhin, Diffusion tensor imaging of the corpus callosum in healthy aging: Investigating higher order polynomial regression modelling, Neuroimage 213 (2020), 116675.
[118] S.K. Song, S.W. Sun, M.J. Ramsbottom, C. Chang, J. Russell, A.H. Cross, Dysmyelination revealed through MRI as increased radial (but unchanged axial) diffusion of water, Neuroimage 17 (3) (2002) 1429–1436.
[119] Y. Pang, L. Campbell, B. Zheng, L. Fan, Z. Cai, P. Rhodes, Lipopolysaccharide-activated microglia induce death of oligodendrocyte progenitor cells and impede their development, Neuroscience 166 (2) (2010) 464–475.
[120] A. Sierra, T. Laitinen, O. Gröhn, A. Pitkänen, Diffusion tensor imaging of hippocampal network plasticity, Brain Struct. Funct. 220 (2) (2015) 781–801.
[121] K. Göbel-Guéniot, J. Gerlach, R. Kamberger, J. Leupold, D. von Elverfeldt, J. Hennig, J.G. Korvink, C.A. Haas, P. LeVan, Histological correlates of diffusion-weighted magnetic resonance microscopy in a mouse model of mesial temporal lobe epilepsy, Front. Neurosci. 14 (2020) 543.
[122] R.A. Salo, T. Miettinen, T. Laitinen, O. Gröhn, A. Sierra, Diffusion tensor MRI shows progressive changes in the hippocampus and dentate gyrus after status epilepticus in rat – histological validation with Fourier-based analysis, Neuroimage 152 (2017) 221–236.
[123] R.A. Salo, I. Belevich, E. Manninen, E. Jokitalo, O. Gröhn, A. Sierra, Quantification of anisotropy and orientation in 3D electron microscopy and diffusion tensor imaging in injured rat brain, Neuroimage 172 (2018) 404–414.
[124] S. Maren, W.G. Holt, Hippocampus and pavlovian fear conditioning in rats: muscimol infusions into the ventral, but not dorsal, hippocampus impair the acquisition of conditional freezing to an auditory conditional stimulus, Behav. Neurosci. 118 (1) (2004) 97–110.
[125] J.J. Quinn, H.M. Wied, Q.D. Ma, M.R. Tinsley, M.S. Fanselow, Dorsal hippocampus involvement in delay fear conditioning depends upon the strength of the tone-footshock association, Hippocampus 18 (7) (2008) 640–654.
[126] T. Bast, W.N. Zhang, J. Feldon, Dorsal hippocampus and classical fear conditioning to tone and context in rats: effects of local NMDA-receptor blockade and stimulation, Hippocampus 13 (6) (2003) 657–675.
[127] B.F. Osborne, S.B. Beamish, J.M. Schwarz, The effects of early-life immune activation on microglia-mediated neuronal remodeling and the associated ontogeny of hippocampal-dependent learning in juvenile rats, Brain Behav. Immun. 96 (2021) 239–255.
[128] J.M. Schwarz, S.D. Bilbo, LPS elicits a much larger and broader inflammatory response than Escherichia coli infection within the hippocampus of neonatal rats, Neurosci. Lett. 497 (2) (2011) 110–115.
[129] U. Meyer, M. Nyffeler, B.K. Yee, I. Knuesel, J. Feldon, Adult brain and behavioral pathological markers of prenatal immune challenge during early/middle and late fetal development in mice, Brain, Behav., Immun. 22 (4) (2008) 469–486.
[130] E.M. Harre, M.A. Galic, A. Mouihate, F. Noorbakhsh, Q.J. Pittman, Neonatal inflammation produces selective behavioural deficits and alters N-methyl-D-aspartate receptor subunit mRNA in the adult rat brain, Eur. J. Neurosci. 27 (3) (2008) 644–653.
[131] C.R. Pierson, R.D. Folkerth, S.S. Billiards, F.L. Trachtenberg, M.E. Drinkwater, J. J. Volpe, H.C. Kinney, Gray matter injury associated with periventricular leukomalacia in the premature infant, Acta Neuropathol. 114 (6) (2007) 619–631.
[132] U.C. Joashi, K. Greenwood, D.L. Taylor, M. Kozma, N.D. Mazarakis, A. D. Edwards, H. Mehmet, Poly(ADP ribose) polymerase cleavage precedes neuronal death in the hippocampus and cerebellum following injury to the developing rat forebrain, Eur. J. Neurosci. 11 (1) (1999) 91–100.
[133] R. Gussenhoven, R.J.J. Westerlaken, D. Ophelders, A.H. Jobe, M.W. Kemp, S. G. Kallapur, L.J. Zimmermann, P.T. Sangild, S. Pankratova, P. Gressens, B. W. Kramer, B. Fleiss, T. Wolfs, Chorioamnionitis, neuroinflammation, and injury: timing is key in the preterm ovine fetus, J. Neuroinflamm. 15 (1) (2018) 113.
[134] K. Hikishima, K. Ando, R. Yano, K. Kawai, Y. Komaki, T. Inoue, T. Itoh, M. Yamada, S. Momoshima, H.J. Okano, H. Okano, Parkinson disease: diffusion mr imaging to detect nigrostriatal pathway loss in a marmoset model treated with 1-methyl-4-phenyl-1,2,3,6-tetrahydropyridine, Radiology 275 (2) (2015) 430–437.
[135] D. Alicata, L. Chang, C. Cloak, K. Abe, T. Ernst, Higher diffusion in striatum and lower fractional anisotropy in white matter of methamphetamine users, Psychiatry Res. 174 (1) (2009) 1–8.
[136] P.J. Winklewski, A. Sabisz, P. Naumczyk, K. Jodzio, E. Szurowska, A. Szarmach, Understanding the physiopathology behind axial and radial diffusivity changes—what do we know? Front. Neurol. 9 (92) (2018).
[137] V.R. Karolis, S. Froudist-Walsh, J. Kroll, P.J. Brittain, C.-E.J. Tseng, K.-W. Nam, A. A.T.S. Reinders, R.M. Murray, S.C.R. Williams, P.M. Thompson, C. Nosarti, Volumetric grey matter alterations in adolescents and adults born very preterm suggest accelerated brain maturation, Neuroimage 163 (2017) 379–389.
[138] W.Y. Loh, P.J. Anderson, J.L.Y. Cheong, A.J. Spittle, J. Chen, K.J. Lee, C. Molesworth, T.E. Inder, A. Connelly, L.W. Doyle, D.K. Thompson, Longitudinal growth of the basal ganglia and thalamus in very preterm children, Brain Imaging Behav. 14 (4) (2020) 998–1011.
[139] C. Nosarti, E. Giouroukou, E. Healy, L. Rifkin, M. Walshe, A. Reichenberg, X. Chitnis, S.C. Williams, R.M. Murray, Grey and white matter distribution in very preterm adolescents mediates neurodevelopmental outcome, Brain 131 (1) (2008) 205–217.
[140] K. Schadl, R. Vassar, K. Cahill-Rowley, K.W. Yeom, D.K. Stevenson, J. Rose, Prediction of cognitive and motor development in preterm children using exhaustive feature selection and cross-validation of near-term white matter microstructure, Neuroimage Clin. 17 (2018) 667–679.
[141] S.V. Sizonenko, E.J. Camm, J.R. Garbow, S.E. Maier, T.E. Inder, C.E. Williams, J. J. Neil, P.S. Huppi, Developmental changes and injury induced disruption of the radial organization of the cortex in the immature rat brain revealed by in vivo diffusion tensor MRI, Cereb. Cortex 17 (11) (2007) 2609–2617.
[142] J.D. Prasad, Y. van de Looij, K.C. Gunn, S.M. Ranchhod, P.B. White, M.J. Berry, L. Bennet, S.V. Sizonenko, A.J. Gunn, J.M. Dean, Long-term coordinated microstructural disruptions of the developing neocortex and subcortical white matter after early postnatal systemic inflammation, Brain Behav. Immun. 94 (2021) 338–356.
[143] H.-P. Müller, D. Brenner, F. Roselli, D. Wiesner, A. Abaei, M. Gorges, K.M. Danzer, A.C. Ludolph, W. Tsao, P.C. Wong, V. Rasche, J.H. Weishaupt, J. Kassubek, Longitudinal diffusion tensor magnetic resonance imaging analysis at the cohort level reveals disturbed cortical and callosal microstructure with spared corticospinal tract in the TDP-43G298S ALS mouse model, Transl. Neurodegener. 8 (1) (2019) 27.
[144] J.M. Dean, Y. van de Looij, S.V. Sizonenko, G.A. Lodygensky, F. Lazeyras, H. Bolouri, I. Kjellmer, P.S. Huppi, H. Hagberg, C. Mallard, Delayed cortical impairment following lipopolysaccharide exposure in preterm fetal sheep, Ann. Neurol. 70 (5) (2011) 846–856.
[145] E. van Tilborg, C.M. van Kammen, C.G.M. de Theije, M.P.A. van Meer, R. M. Dijkhuizen, C.H. Nijboer, A quantitative method for microstructural analysis of myelinated axons in the injured rodent brain, Sci. Rep. 7 (1) (2017) 16492.
[146] J.L. Cheong, D.K. Thompson, H.X. Wang, R.W. Hunt, P.J. Anderson, T.E. Inder, L. W. Doyle, Abnormal white matter signal on MR imaging is related to abnormal tissue microstructure, AJNR Am. J. Neuroradiol. 30 (3) (2009) 623–628.
[147] S.J. Counsell, Y. Shen, J.P. Boardman, D.J. Larkman, O. Kapellou, P. Ward, J. M. Allsop, F.M. Cowan, J.V. Hajnal, A.D. Edwards, M.A. Rutherford, Axial and radial diffusivity in preterm infants who have diffuse white matter changes on magnetic resonance imaging at term-equivalent age, Pediatrics 117 (2) (2006) 376–386.
[148] A. Jurcoane, M. Daamen, L. Scheef, J.G. Bäuml, C. Meng, A.M. Wohlschläger, C. Sorg, B. Busch, N. Baumann, D. Wolke, P. Bartmann, E. Hattingen, H. Boecker, White matter alterations of the corticospinal tract in adults born very preterm and/or with very low birth weight, Hum. Brain Mapp. 37 (1) (2016) 289–299.
[149] E. Kennedy, T. Poppe, A. Tottman, J. Harding, Neurodevelopmental impairment is associated with altered white matter development in a cohort of school-aged children born very preterm, Neuroimage Clin. 31 (2021), 102730.

[150] R.H. Leuchter, L. Gui, A. Poncet, C. Hagmann, G.A. Lodygensky, E. Martin, B. Koller, A. Darque, H.U. Bucher, P.S. Huppi, Association between early administration of high-dose erythropoietin in preterm infants and brain MRI abnormality at term-equivalent age, JAMA 312 (8) (2014) 817–824.
[151] M. Rutherford, L.A. Ramenghi, A.D. Edwards, P. Brocklehurst, H. Halliday, M. Levene, B. Strohm, M. Thoresen, A. Whitelaw, D. Azzopardi, Assessment of brain tissue injury after moderate hypothermia in neonates with hypoxic–ischaemic encephalopathy: a nested substudy of a randomised controlled trial, Lancet Neurol. 9 (1) (2010) 39–45.
[152] Y.W. Wu, A.M. Goodman, T. Chang, S.B. Mulkey, F.F. Gonzalez, D.E. Mayock, S. E. Juul, A.M. Mathur, K. Van Meurs, R.C. McKinstry, R.W. Redline, Placental pathology and neonatal brain MRI in a randomized trial of erythropoietin for hypoxic-ischemic encephalopathy, Pediatr. Res. 87 (5) (2020) 879–884.
[153] H.W. Chung, C.Y. Chen, R.A. Zimmerman, K.W. Lee, C.C. Lee, S.C. Chin, T2-Weighted fast MR imaging with true FISP versus HASTE: comparative efficacy in the evaluation of normal fetal brain maturation, AJR Am. J. Roentgenol. 175 (5) (2000) 1375–1380.
[154] F. Edris, A. Kielar, K.F. Fung, L. Avruch, M. Walker, Ultrasound and MRI in the antenatal diagnosis of schizencephaly, J. Obstet. Gynaecol. Can. 27 (9) (2005) 864–868.
[155] N. Merchant, D. Azzopardi, S. Counsell, P. Gressens, A. Dierl, I. Gozar, A. Kapetanakis, M. Wan, G. Ball, M. Rutherford, M. Sharma, J. Allsop, M. Fox, B. Jani, S. Palaniappan, I. Bisson, A. Edwards, O-057melatonin as a novel neuroprotectant in preterm infants – a double blinded randomised controlled trial (mint study), Arch. Dis. Child. 99 (2) (2014) A43.2–A43. A43-A43.
[156] R.L. O'Gorman, H.U. Bucher, U. Held, B.M. Koller, P.S. Hüppi, C.F. Hagmann, E.P. O.N.T.G. the Swiss, Tract-based spatial statistics to assess the neuroprotective effect of early erythropoietin on white matter development in preterm infants, Brain 138 (2) (2015) 388–397.
[157] T. Poppe, B. Thompson, J.P. Boardman, M.E. Bastin, J. Alsweiler, G. Deib, J. E. Harding, C.A. Crowther, Effect of antenatal magnesium sulphate on MRI biomarkers of white matter development at term equivalent age: the magnum study, EBioMedicine 59 (2020), 102957.
[158] A. Jakab, C. Ruegger, H.U. Bucher, M. Makki, P.S. Huppi, R. Tuura, C. Hagmann, Network based statistics reveals trophic and neuroprotective effect of early high dose erythropoetin on brain connectivity in very preterm infants, NeuroImage: Clin. 22 (2019), 101806.
[159] Y. Wang, Q. Wang, J.P. Haldar, F.C. Yeh, M. Xie, P. Sun, T.W. Tu, K. Trinkaus, R. S. Klein, A.H. Cross, S.K. Song, Quantification of increased cellularity during inflammatory demyelination, Brain 134 (12) (2011) 3590–3601.
[160] A.H. Cross, S.K. Song, A new imaging modality to non-invasively assess multiple sclerosis pathology, J. Neuroimmunol. 304 (2017) 81–85.
[161] X. Wang, M.F. Cusick, Y. Wang, P. Sun, J.E. Libbey, K. Trinkaus, R.S. Fujinami, S. K. Song, Diffusion basis spectrum imaging detects and distinguishes coexisting subclinical inflammation, demyelination and axonal injury in experimental autoimmune encephalomyelitis mice, NMR Biomed. 27 (7) (2014) 843–852.
[162] S. Schiavi, M. Petracca, P. Sun, L. Fleysher, S. Cocozza, M.M. El Mendili, A. Signori, J.S. Babb, K. Podranski, S.K. Song, M. Inglese, Non-invasive quantification of inflammation, axonal and myelin injury in multiple sclerosis, Brain 144 (1) (2021) 213–223.
[163] Z. Ye, K. Srinivasa, A. Meyer, P. Sun, J. Lin, J.D. Viox, C. Song, A.T. Wu, S.K. Song, S. Dahiya, J.B. Rubin, Diffusion histology imaging differentiates distinct pediatric brain tumor histology, Sci. Rep. 11 (1) (2021) 4749.
[164] Z. Ye, R.L. Price, X. Liu, J. Lin, Q. Yang, P. Sun, A.T. Wu, L. Wang, R.H. Han, C. Song, R. Yang, S.E. Gary, D.D. Mao, M. Wallendorf, J.L. Campian, J.S. Li, S. Dahiya, A.H. Kim, S.K. Song, Diffusion histology imaging combining diffusion basis spectrum imaging (DBSI) and machine learning improves detection and classification of glioblastoma pathology, Clin. Cancer Res. 26 (20) (2020) 5388–5399.
[165] H. Zhang, T. Schneider, C.A. Wheeler-Kingshott, D.C. Alexander, NODDI: practical in vivo neurite orientation dispersion and density imaging of the human brain, Neuroimage 61 (4) (2012) 1000–1016.
[166] Z. Eaton-Rosen, A. Melbourne, E. Orasanu, M.J. Cardoso, M. Modat, A. Bainbridge, G.S. Kendall, N.J. Robertson, N. Marlow, S. Ourselin, Longitudinal measurement of the developing grey matter in preterm subjects using multi-modal MRI, Neuroimage 111 (2015) 580–589.
[167] I.O. Jelescu, J. Veraart, V. Adisetiyo, S.S. Milla, D.S. Novikov, E. Fieremans, One diffusion acquisition and different white matter models: how does microstructure change in human early development based on WMTI and NODDI? Neuroimage 107 (2015) 242–256.
[168] D. Batalle, J. O'Muircheartaigh, A. Makropoulos, C.J. Kelly, R. Dimitrova, E. J. Hughes, J.V. Hajnal, H. Zhang, D.C. Alexander, A.D. Edwards, S.J. Counsell, Different patterns of cortical maturation before and after 38 weeks gestational age demonstrated by diffusion MRI in vivo, Neuroimage 185 (2019) 764–775.
[169] G. Ball, J. Seidlitz, J. O'Muircheartaigh, R. Dimitrova, D. Fenchel, A. Makropoulos, D. Christiaens, A. Schuh, J. Passerat-Palmbach, J. Hutter, L. Cordero-Grande, E. Hughes, A. Price, J.V. Hajnal, D. Rueckert, E.C. Robinson, A.D. Edwards, Cortical morphology at birth reflects spatiotemporal patterns of gene expression in the fetal human brain, PLoS Biol. 18 (11) (2020), e3000976.
[170] L.T. Tien, Y.J. Lee, Y. Pang, S. Lu, J.W. Lee, C.H. Tseng, A.J. Bhatt, R.D. Savich, L. W. Fan, Neuroprotective effects of intranasal IGF-1 against neonatal lipopolysaccharide-induced neurobehavioral deficits and neuronal inflammation in the substantia nigra and locus coeruleus of juvenile rats, Dev. Neurosci. 39 (6) (2017) 443–459.